AD-A230 623

UNIVERSITY OF SOUTHERN CALIFORNIA
SCHOOL OF ENGINEERING

FILE COPY

JOINT SERVICES ELECTRONICS PROGRAM
RESEARCH IN ELECTRONICS

F49620-88-C-0067

THIRD ANNUAL TECHNICAL REPORT

FOR THE PERIOD
January 1, 1990 through December 31, 1990

Presented to:

The Air Force Office of Scientific Research
Building 410
Bolling Air Force Base, DC 20332

DTIC
ELECTE
JAN 0 3 1991
S D
D

Presented by:

University of Southern California
Electronic Sciences Laboratory
LOS ANGELES, CALIFORNIA 90089-0483

DISTRIBUTION STATEMENT A
Approved for public release
Distribution Unlimited

REPORT DOCUMENTATION PAGE

Form Approved
OMB No. 0704-0188

Public reporting burden for this collection of information is estimated to average 1 hour per response, including the time for reviewing instructions, searching existing data sources, gathering and maintaining the data needed, and completing and reviewing the collection of information. Send comments regarding this burden estimate or any other aspect of this collection of information, including suggestions for reducing this burden, to Washington Headquarters Services, Directorate for information Operations and Reports, 1215 Jefferson Davis Highway, Suite 1204, Arlington, VA 22202-4302, and to the Office of Management and Budget, Paperwork Reduction Project (0704-0188), Washington, DC 20503.

1. AGENCY USE ONLY (Leave blank)	2. REPORT DATE	3. REPORT TYPE AND DATES COVERED
	January 5, 1991	THIRD ANNUAL TECHNICAL REPORT 1/1/90--12/31/90

4. TITLE AND SUBTITLE
JOINT SERVICES ELECTRONICS PROGRAM IN ELECTRONICS

5. FUNDING NUMBERS

6. AUTHOR(S)
WILLIAM H. STEIER

7. PERFORMING ORGANIZATION NAME(S) AND ADDRESS(ES)
UNIVERSITY OF SOUTHERN CALIFORNIA
UNIVERSITY PARK
LOS ANGELES, CA 90089-0483

8. PERFORMING ORGANIZATION REPORT NUMBER

9. SPONSORING/MONITORING AGENCY NAME(S) AND ADDRESS(ES)
AFOSR
BUILDING 410
BOLLING AIR FORCE BASE, DC 20332

10. SPONSORING/MONITORING AGENCY REPORT NUMBER
F49620-88-C0067

11. SUPPLEMENTARY NOTES

12a. DISTRIBUTION/AVAILABILITY STATEMENT

12b. DISTRIBUTION CODE

13. ABSTRACT (Maximum 200 words)

This report documents the progress made on the 13 research topics supported by the Joint Services Electronics Program for the period 1/1/90 through 12/31/90. There are four research topics is solid state electronics, four in quantum electronics, and five in information electronics.

14. SUBJECT TERMS
Electronic Material, Semiconductors, Quantum Electronics, Lasers, communications, Signal Processing, Computers, Controls.

15. NUMBER OF PAGES
74

16. PRICE CODE

17. SECURITY CLASSIFICATION OF REPORT	18. SECURITY CLASSIFICATION OF THIS PAGE	19. SECURITY CLASSIFICATION OF ABSTRACT	20. LIMITATION OF ABSTRACT

90 12 26 187

UNIVERSITY OF SOUTHERN CALIFORNIA

JOINT SERVICES ELECTRONICS PROGRAM
RESEARCH IN ELECTRONICS

F49620-88-C-0067

THIRD ANNUAL TECHNICAL REPORT

FOR THE PERIOD
January 1, 1990 through December 31, 1990

Presented to:

The Air Force Office of Scientific Research
Building 410
Bolling Air Force Base, DC 20332

Presented by:

University of Southern California
Electronic Sciences Laboratory
LOS ANGELES, CALIFORNIA 90089-0483

Accession For
NTIS GRA&I
DTIC TAB
Unannounced
Justification
By per AD-A217745
Distribution /
Availability Codes
Dist | Avail and/or Special
A-1

TABLE OF CONTENTS

DIRECTORS OVERVIEW

This report summarizes the progress made under the Joint Services Electronics Program for the period 1 January 1990 through 31 December 1990. This is the third annual technical report under contract F49620-88-C-0067 and covers the thirteen research units supported; four in solid state electronic, four in quantum electronics, and five in information electronics.

Scientific publications and graduating students are the primary output of this research and are a good indication of the progress made. During this period 48 scientific publications have appeared in print, been presented, or have been submitted. One PhD thesis was completed under the JSEP support of Prof. Sawchuk.

Each of the thirteen research units have documented significant research progress during this period but two units have made progress that warrants special emphasis.

I. Selective Area Epitaxy Growth of Photonic Device Structures by MOCVD - P. D. Dapkus

Prof Dapkus and his students have demonstrated that laser assisted atomic layer epitaxy of GaAs is a promising new approach to fabricating photonic circuits and devices. Alternate single atomic layers of Ga and As can be grown and at the same time circuits and devices can be patterned by a laser. The alternating layers are grown by rotating the sample from one chamber to another and the transverse pattern is controlled by a focused laser beam at 5145 Å. In these preliminary experiments patterns of 20μm dimensions were written.

II. Optoelectronic and Quantum Structures Using Pristine and Irradiated Organic Compounds - S. R. Forrest

During this period Prof Forrest and his students have made significant progress in the organic MBE deposition of very high optical and electronic quality films of the crystalline organic PTCDA. These films have numerous applications in optoelectronic and optical devices. The material quality has been demonstrated by the very low loss propagation in ridge waveguides; <2.5 dB/cm at 1.06 and at 1.3μm. These films also show a very large amount of birefringence which makes several novel new devices possible. From the waveguiding experiments the TE index of refraction was measured to be 2.017 and from other optical measurements the TM index as found to be 1.35

Selective Area Epitaxy Growth of Photonic Device Structures by Metalorganic Chemical Vapor Deposition (MOCVD)

P.D. Dapkus

PROGRESS

During this period we have undertaken three activities: studies of laser assisted growth of GaAs, studies of the use of alternate As sources for MOCVD and ALE growth, and studies of growth and characterization of strained layer InGaAs/GaAs structures.

LASER ASSISTED ALE OF GaAs

Our goal in this portion of the program has been to determine the limits to the spatial resolution of LALE and the mechanisms controlling this resolution. We have previously demonstrated stripes as narrow as 20μm could be deposited with a tightly focussed 5145 Å beam. This work was done in a multi-chambered reactor in which the sample was alternately exposed to trimethylgallium (TMGa), H_2, AsH_3, and H_2 by rotating the sample from one chamber to another. The laser is incident on the sample (as the sample is scanned past the focal point of the beam) only during a portion of the TMGa exposure. The system is equipped with a stepper motor to allow a variation of the angular speed at any point during the deposition. In our initial experiments to determine the resolution limit by focussing the beam to a smaller spot with this system, we determined that this approach nad several flaws. First, the narrower the focal spot of the laser the shorter was the laser exposure time to achieve saturated growth at a given power. In addition, the higher intensities required to achieve growth under these condition created defects in the material suggesting that a strong thermal component was operative under these conditions. It also became difficult to determine the laser spot size owing to the geometry of the reactor and thermal effects in the gas phase. The greatest difficulty, however, arose in evaluating the material. Since the growth rates that are achievable by this process are low, it is impractical to grow more than one stripe in a given growth run. Thus, the location of the laser grown stripe is often difficult to locate for PL evaluation and too small to evaluate by C-V techniques. As a result of these difficulties, we decided to adopt a new experimental strategy utilizing a higher power laser to achieve large area growth. Our approach to determine the resolution limits is then to project patterns of different geometry on the

surface to determine the spatial resolution of the process. To this end we purchased a high power Ar ion laser and designed a new reactor geometry that would allow us to project more complex patterns on to a stationary wafer. The laser is in place and the parameters for growth of large size stripes in our rotating reactor has been thoroughly investigated. In fact, we determined that very high quality GaAs materials can be grown by LALE and that high quality heterojunctions can be fabricated in the same growth run by growing the AlGaAs layers by conventional MOCVD in one of the H_2 chambers and the GaAs layer by LALE. A new reactor design that allows all the layers to be grown in the same chamber with a stationary substrate has been designed and received.

These experiments will undergo intensive effort over the next several months so that we can capitalize on results achieved in the rotating reactor. These results were partially funded through a contract from SDIO/IST and administered by ARO and by our ONR contract. We have optimized the properties of LALE grown GaAs using the rotating reactor design. This has resulted in the demonstration of the first heterojunction device grown by LALE. The data of Fig. 1 show the threshold current density and emission wavelength of 30μm wide stripe geometry quantum well lasers fabricated from a wafer with a large area quantum well region grown by LALE. The variation of the emission wavelength across the LALE grown region is apparent in the figure. The lowest threshold current is 650A/cm^2 and occurs in the center of the stripe. This is threshold is a factor of 2.5-3.0 greater than has been achieved with conventional MOCVD. Work is continuing to improve the performance of these devices and to incorporate them into more complex geometries. Determining the spatial resolution now is of prime importance in assessing the importance if this approach for a range of applications.

MOCVD GROWTH USING AsH_3 ALTERNATIVES

The low temperature at which LALE is carried out (<400°C) creates some difficulty in terms of the amount of AsH_3 required in the growth process. AsH_3 does not decomposed efficiently at these low temperatures. As a result an alternative to AsH_3 that cracks at lower temperature is desirable. In addition, the extreme toxicity of AsH_3 is an issue of increasing concern in the academic environment. For these reasons, we undertook a study of the growth of AlGaAs/GaAs structures using tertiarybutylarsine and monoethylarsine. These materials were provided to us by the manufacturers (American Cyanamid (TBAs) and Alfa Ventron (MEAs)) free of charge for these studies. The results of these studies are

most encouraging. We have determined that high quality GaAs, AlGaAs, and AlGaAs/GaAs heterostructures can be grown with TBAs. Our studies with MEAs are also encouraging but not as far along.

We have demonstrated that high purity GaAs, high quantum efficiency AlGaAs and AlGaAs/GaAs quantum wells can be grown with TBAs. The luminescence efficiency of the quantum wells is comparable to AsH_3 grown material and exhibits a narrow PL linewidth at low temperatures. Most important, however, is the fact that the minority carrier lifetime of the TBAs grown heterostructures was comparable to AsH_3 grown materials grown in the same reactor. A minority carrier lifetime of 400 ns was achieved for sample consisting of a 2μm thick GaAs layer sandwiched by 30% AlGAs when TBAs was used for the entire structure. A lifetime of 1ms has been achieved under optimum conditions with AsH_3. As confirmation of the quality of these materials a quantum well laser structure was grown that exhibited laser thresholds as low as 400 A/cm^2. This threshold is approximately 50% higher than would be observed for AsH_3 grown devices of the same length. It is noteworthy that these results are the first to demonstrate device quality materials with AsH_3 alternatives and open the way for a safer MOCVD process and for lower utilization of AsH_3 in LALE.

InGaAs/GaAs STRAINED LAYER MATERIALS

Reduced threshold lasers are being achieved with InGaAs strained layer lasers because of the lower in-plane effective mass that results from the incorporation of strain in the layers. Already several laboratories have demonstrated low threshold and excellent reliability for these devices and some have incorporated strained layer active regions in vertical cavity surface emitting lasers. We asked the question: how much strain can be incorporated in these structures before misfit dislocations are formed and what is the effect of strain on properties such as the laser threshold and the conduction band offset? The last issue is of importance for modelling the laser threshold and predicting the ultimate performance potential of these structures.

We have developed a methodology for characterizing the thin strained layers required for laser applications. The limits placed on the thickness and In composition of InGaAs layer grown on GaAs substrates are determined by the elastic strain limit of the material. At a given composition this limit defines a critical thickness beyond which misfit dislocations are formed. Models, although not accurately describing

experiments, suggest maximum thicknesses for coherent layers that make difficult the determination of even such a basic parameter as In concentration. The composition of layer is usually determined by X-ray measurements on thick, "relaxed" layers grown under the same conditions as the strained layers. Disregarding the possible effects of strain on growth kinetics, such measurements rely critically on the complete relaxation of strain by the formation of misfit dislocations. Partial relaxation will result in inaccuracies of magnitude comparable to the residual strain, i.e. 90% relaxation instead of complete relaxation will result in a 10% error in the measured In concentration. To circumvent this problem we have developed a methodology based upon double crystal X-ray diffractometry (DCXD) that allows us to characterize single strained quantum wells in as-grown samples. The technique relies on the observation of Pendollosung fringes in the DCXD rocking curve from multilayers containing strained layers. An example of a rocking curve from samples containing three strained InGaAs quantum wells on a GaAs substrate is shown in Figure 2. The rich array of diffraction fringes present in this data result from X-ray interference effects in the multilayer sample. To interpret these data we have develop a program based on the dynamic theory of X-ray scattering which allows us to model the diffraction expected from a specified sample. In our work we fit the experimental data by varying the layer thicknesses and compositions until a best fit is obtained. The dotted curve in the figure shows the theoretical fit chosen for this particular sample. We are able to determine the layer thickness of strained quantum wells to within one monolayer and the In composition to within 0.5% absolute. Verification of the layer thicknesses has been accomplished by cross-sectional TEM and the In composition accuracy is estimated by the sensitivity of the model to In composition. This approach has allowed us to nondestructively characterize strained quantum well structures with layer thicknesses as small as 30Å.

This methodolgy has also allowed us to determine the conduction and valence band offsets in InGaAs/GaAs structures by measuring the luminescence transition energy of well characterized quantum well samples. By measuring a wide range of samples with varying quantum well widths and compositions we have been able to fit the data using a square well potential model and determine that the conduction band offset, ΔE_C, is 0.6 of the total energy band difference, ΔE_g, i.e. $\Delta E_C = (0.60 \pm 0.03) \times \Delta E_g$. This value agrees well with values determined from InGaAs/GaAs 2D hole gas measurements (0.63) and is the first unambiguous optical determination of this critical parameter.

The issues determining the onset of misfit dislocations have grown in importance since the work of Fitzgerald demonstrated that for low In compositions (<5%), the nucleation of misfits is kinetically controlled. This had also been suggested by Madhukar based upon Monte Carlo simulations of the growth of strained layers. We undertook a study of the effects of growing strained layers on nonplanar regions of GaAs substrates to determine the effects of limited area growth on the inhibition of misfit formation. By growing on features smaller than the average separation between defects, a considerable suppression of misfit formation may be obtained and layer thicknesses in excess of the critical thickness on planar substrates could be achieved. Motivated by our previous work on low threshold lasers grown on nonplanar substrates, we explored the growth of InGaAs(20% In) layers of various thicknesses on GaAs substrates with mesas etched along the <110> and <$\bar{1}$10> directions. The onset of misfit dislocation formation was monitored by measuring the PL efficiency of the samples for the different layer thicknesses. Fig. 3 shows PL efficiency of these samples for mesas oriented along the <110> direction. Note that at some critical thickness, which in the case of the planar samples exceeds the Matthews-Blakeslee model by a factor of two, the PL efficiency drops precipitously owing to the formation of misfit dislocations. Note also that the growth on top of the mesa effectively increases the critical thickness by a factor of 1.5 as compared to the planar samples. Detailed TEM characterization of the samples indicates that the layer thicknesses are accurately predicted by the growth rate in the planar regions for both cases. This observation suggests that even for highly strained layers as are studied here misfit dislocation generation can be inhibited by growth on small area features.

PUBLICATIONS

1. "Thermal and laser assisted atomic layer epitaxy of compound semiconductors", S. P. Denbaars*, P. D. Dapkus, J. S. Osinski*, M. Zandian*, C. A. Beyler*, and K. M. Dzurko*, Proc. of Int. Symp. GaAs and Related Compounds; Inst. Phys. Conf. Ser. No. 96, 89 (1989).

2. "Minority carrier lifetimes in undoped AlGaAs/GaAs quantum wells", A. Hariz*, P. D. Dapkus, H. C. Lee*, E. P. Menu†, and S. P. Denbaars*, Appl. Phys. Lett. **54**, 635 (1989).

3. " Atomic layer epitaxy of GaAs and InAs", W. G. Jeong*, E. P. Menu†, and P. D. Dapkus, Mat. Res. Symp. Proc. **145**, 163 (1989).

4. "Band-edge absorption coefficients from photoluminescence in semiconductor multiple quantum wells" , A. Kost†, H. C. Lee, Yao Zou*, P. D. Dapkus, and E. Garmire, Appl. Phys. Lett. **54,** 1356 (1989).

5. "Atomic Layer epitaxy of compound semiconductors with metalorganic precursors", S. P. DenBaars* and P. D. Dapkus, J. Crystal Growth **98**, 195 (1989).

6. "GaAs based opto-thyristors for pulsed power applications", J. H. Hur*, P. Hadizad*, S. Hummel*, K. M. Dzurko*, P. D. Dapkus, M. A. Gundersen, and H. R. Fetterman, submitted to IEEE Trans. Electron Dev.

7. "Determination of the energy band offsets of GaAs/InGaAs strained layer quantum wells.", Yao Zou*, P. A. Grodzinski*, E. P. Menu†, P. D. Dapkus, J. J. Alwan*, and J. J. Coleman, Submitted to Appl. Phys. Lett.

8. "Growth and Characterization of InGaAs strained layers on GaAs nonplanar substrates". P. A. Grodzinski*, Yao Zou*, J. S. Osinski*, and P. D. Dapkus, Submitted to J. Crystal Growth.

9. "Growth and properties of AlGaAs/GaAs quantum wells and lasers grown by metalorganic chemical vapor deposition using tertiarybutylarsine", S. G. Hummel*, C. A. Beyler*, P. A. Grodzinski*, and P. D. Dapkus, Accepted for publication Appl. Phys Lett.

10. "RHEED and XPS observations of trimethylgallium adsorption on (001) GaAs surfaces - relevance to atomic layer epitaxy", B. Y. Maa* and P. D. Dapkus, Accepted for publication J. Electronic Materials.

11. "Studies of TMGa adsorption on thin GaAs and InAs (001) Layers", B. Y. Maa* and P. D. Dapkus, Accepted for publication J Crystal Growth.

12. "Photoluminescence study of critical thickness of pseudomorphic quantum wells grown on small area mesa stripes", Yao Zou, Piotr Grodzinski, Julian Osinski, and P. D. Dapkus. Submitted for publication in Appl. Phys. Lett.

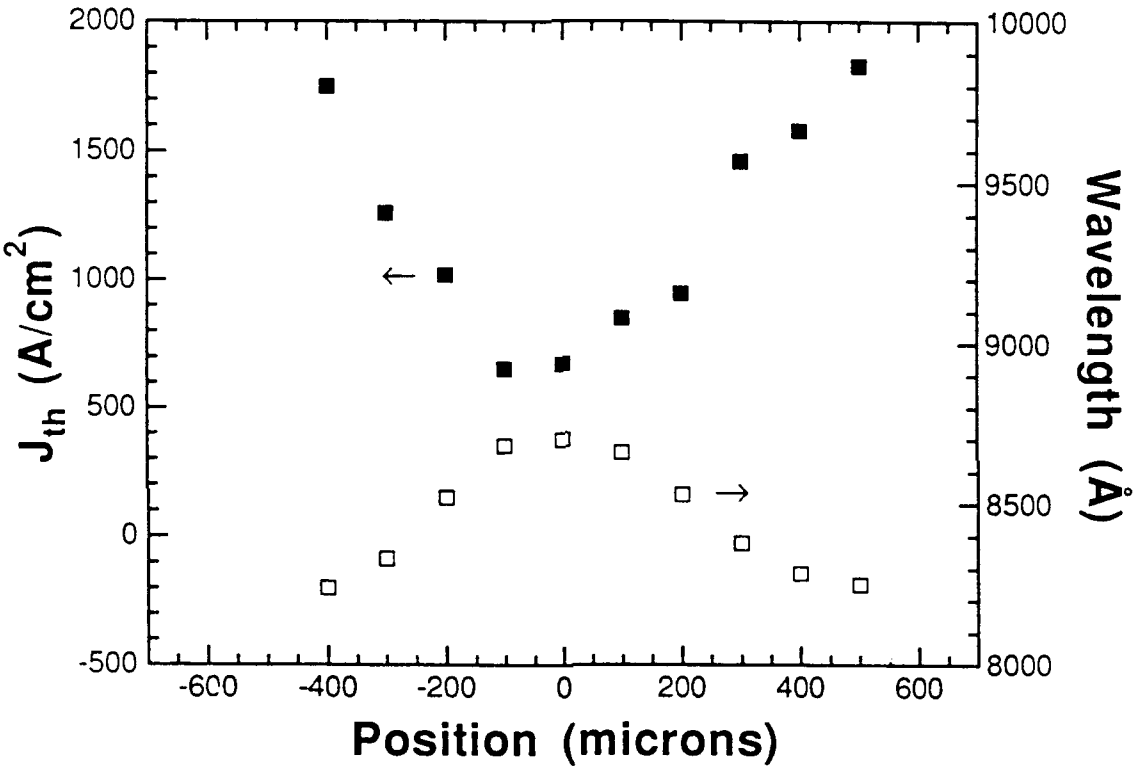

1. Dependence of laser threshold and wavelength as a function of position for a quantum well laser structure with the the active region grown by large spot, laser assisted atomic layer epitaxy.

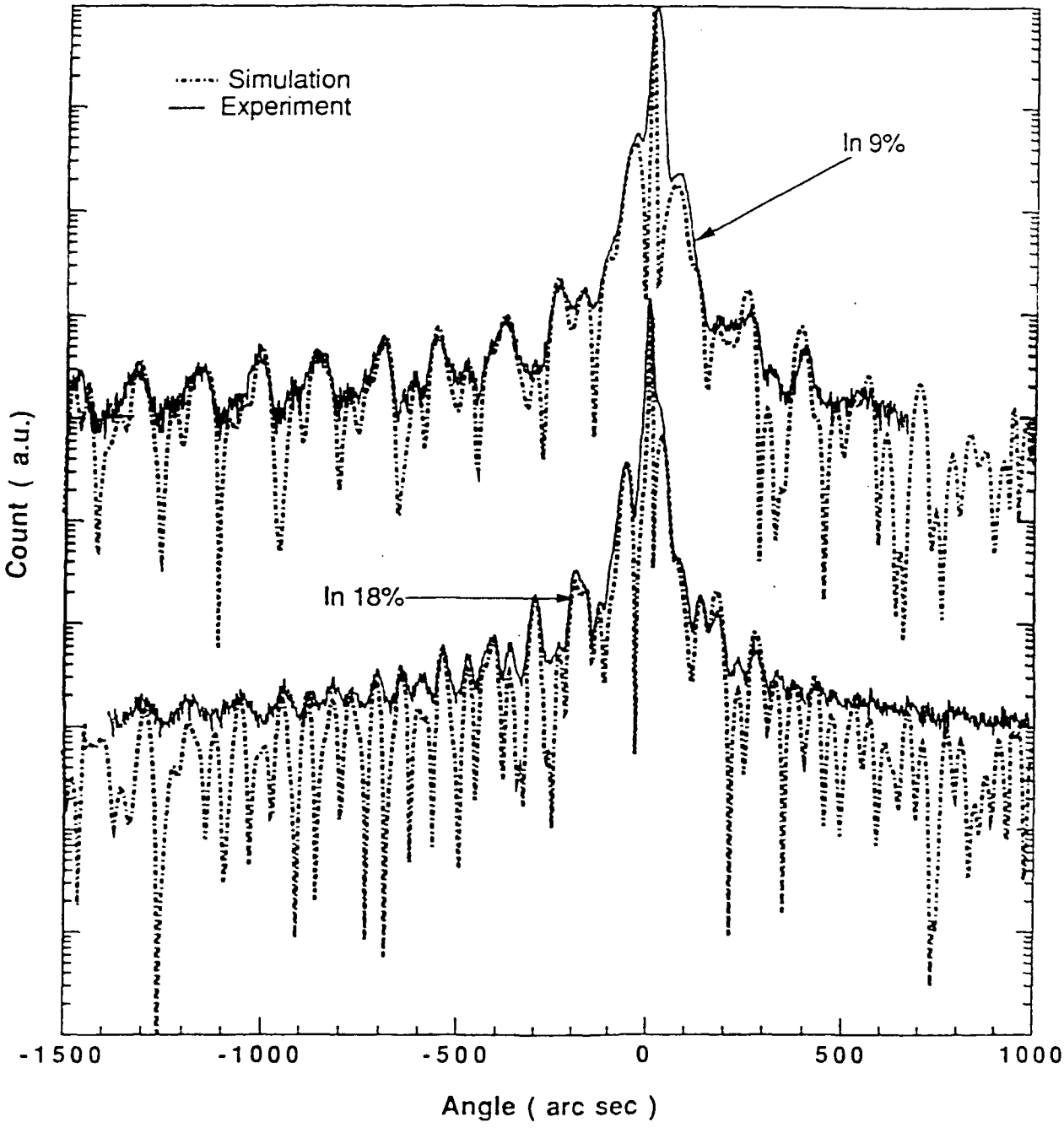

2. Double crystal X-ray diffraction simulation (dotted curves) and experimental data for two quantum well samples containing strained quantum well materials. Each sample contains three QW's with different widths. The match of the simulation and data is excellent.

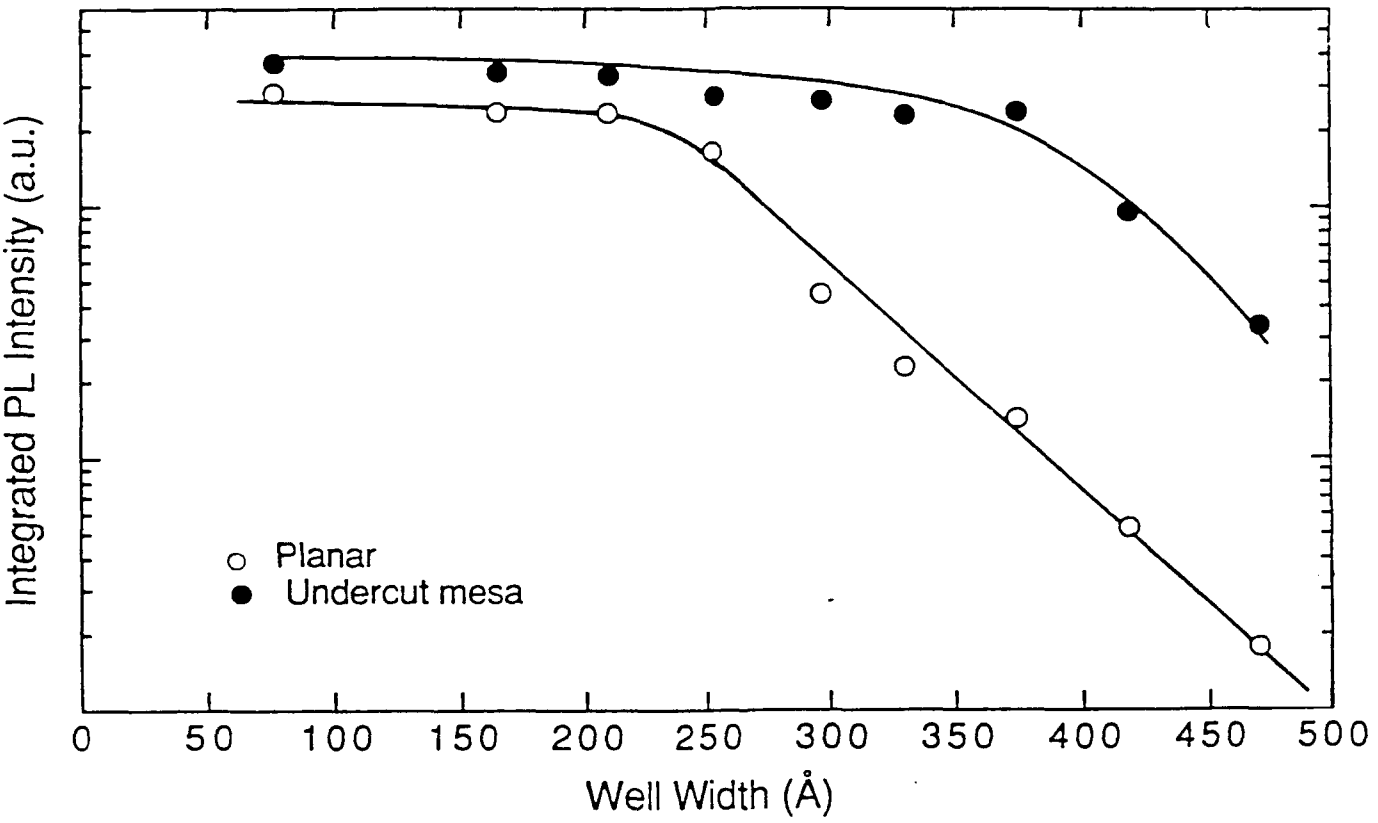

3. Dependence of integrated PL intensity on well width for strained QW's grown on planar (open dots) and structured substrates. Note increase in apparent critical thickness on structured substrates.

Highly Strained $In_xGa_{1-x}As$/AlAs Based Resonant Tunneling Diodes Grown on GaAs Substrates with Simultaneously High Peak to Valley Ratios and Peak Current Densities.

A. Madhukar
SS3-2

PROGRESS

We have succeded in fabricating pseudomorphic resonant tunneling diodes (RTDs) with simultaneously high peak to valley ratios (PVR) and peak current densities (J_p) at room temperature on GaAs (100) substrates. $In_xGa_{1-x}As$/AlAs RTDs on GaAs substrates with PVR of $\sim$ 4 and Jp $\sim$ 10 kA/cm^2 have been realized in the past for $x \leq 0.25$ using conventional strained alloys[1]. But in order to go to higher J_p maintaining a high PVR it is desirable to have a higher conduction band discontinuity requiring the usage of higher x. However, devices with $x \geq 0.3$ have been severely limited by the onset of 3D island growth mode due to the strain ($\Delta a/a \geq 2$ %). The 3D growth mode destroys the highly perfect interfaces required for quantum interference based devices such as RTDs. Using Reflection High Energy Diffraction (RHEED) studies of strained layer $In_xGa_{1-x}As$ epitaxy on GaAs we have been able to identify growth conditions for obtaining layer-by-layer growth for both $(InAs)_M/(GaAs)_N$ short period MQW type well layers and conventional alloys with $x \geq 0.3$.

The RTD structures fabricated were triple-well double-barrier type consisting of an undoped $In_xGa_{1-x}As$ well sandwiched between undoped AlAs barriers, with undoped $In_yGa_{1-y}As$ spacer layers on either side of the tunneling structure. Devices with x = 0.3 or 0.33 grown under non-optimal growth conditions barely showed resonant tunneling. RTD # 28 containing short period MQW strained well layer with equivalent x = 0.33 grown under optimized conditions showed a room temperature PVR of $\sim$ 5 with J_p = 125 kA/cm^2 (fig 1a). The TEM micrograph of this device shown in fig 1b shows highly abrupt interfaces with a layer-by-layer morphology. Similarly RTD # 29 grown using conventional alloy strained well layer with x = 0.3 under optimized conditions gave a room temperature PVR 0f $\sim$ 5 with J_p =

32 kA/cm^2 (fig 1c). Again the TEM micrograph (fig 1d) shows layer-by-layer morphology with abrupt interfaces. The distinguishing characteristic of our devices is that high performance RTDs have been achieved on GaAs substrate without the use of thick strain relieving buffer layers of lattice mismatched materials. These devices are thus suitable for optoelectronic integration on GaAs substrates.

(1) R.Kapre, A.Madhukar, and S.Guha, IEEE Electron Device Lett. 11, p.270, 1990.

PUBLICATIONS

1. R.Kapre, A.Madhukar, K.Kaviani, S.Guha, and K..Rajkumar, "Realization and Anlysis of GaAs/AlAs/In0.1Ga0.9As Based Resonant Tunneling Diodes with High Peak to Valley Ratios at Room Temperature", Appl. Phys. Lett. 56, p.922, 1990.

2. R.Kapre, A.Madhukar, and S.Guha, "$In_{0.25}Ga_{0.75}As$/AlAs Based Resonant Tunneling Diodes Grown on Pre-patterned and Non-patterned GaAs(100) Substrates",IEEE Electron Device Lett. 11p. 270, 1990.

3. R.M.Kapre, A.Madhukar, and S.Guha, "Highly Strained Pseudomorphic $In_XGa_{1-X}As$/AlAs Based Resonant Tunneling Diodes Grown on Patterned and Non-Patterned GaAs (100) Substrates", Proc. of the Sixth International Conference on MBE, Aug 27-31, 1990, San Diego, CA. To appear in Journal of Crystal Growth.

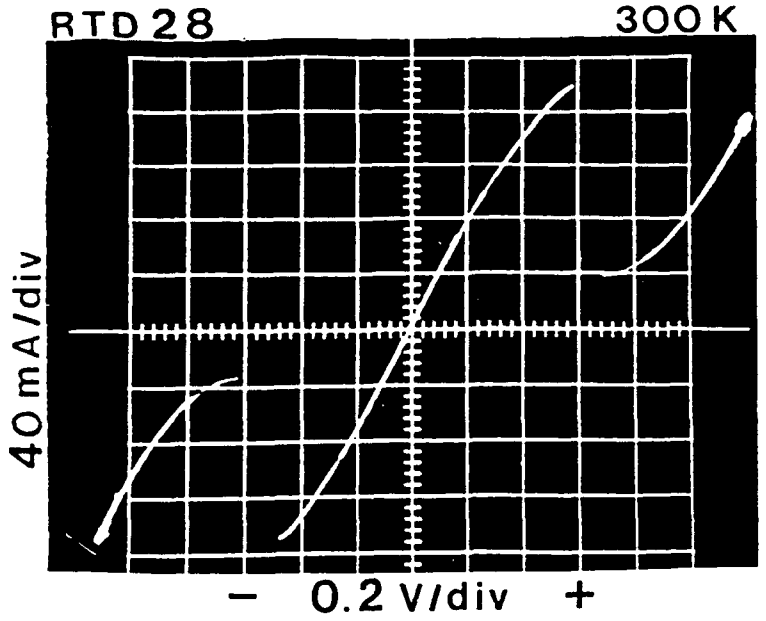

(a)

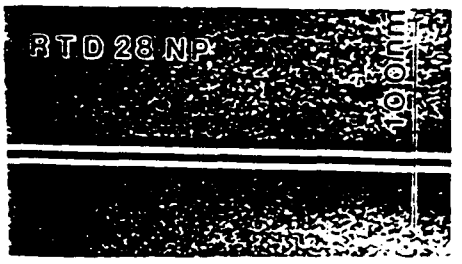

(b)

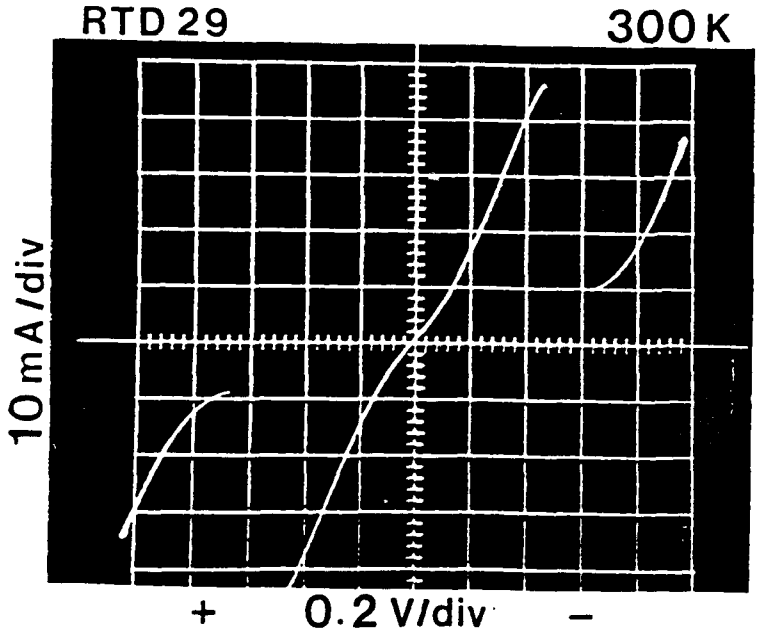

(c)

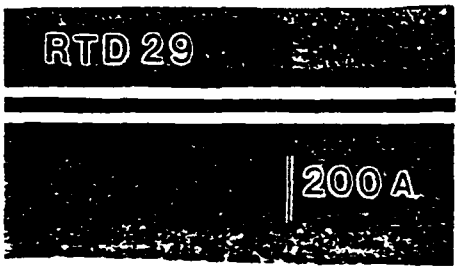

(d)

Figure 1. (a) I-V characteristics of RTD # 28 from 12 μm x 12 μm mesas. (b) Cross sectional TEM micrograph of RTD # 28. (c) I-V characteristics of RTD # 29 from 12 μm x 12 μm mesas. (d) Cross sectional TEM micrograph of RTD # 29.

Electrooptic Devices for Optical Information Processing and Computing Applications

A. R. Tanguay, Jr
SS3-3

PROGRESS

During the current contract period, the primary focus of the research effort has been on further understanding of the fundamental physical processes that characterize the Photorefractive Incoherent-to-Coherent Optical Converter (PICOC) [JSEP Publ. 1], as well as on the optimization of device performance characteristics. The PICOC device is a two-dimensional spatial light modulator that combines photorefractive volume holographic storage principles with erasure by an incoherent image-bearing light source to effect a high resolution incoherent-to-coherent conversion. This particular approach to the development of a viable spatial light modulation technology has been shown to be characterized by relatively high performance, and at the same time is extremely simple in design and hence capable of inexpensive fabrication in a production environment.

A number of key technical issues are under continuing investigation in parallel, including an extensive investigation of PICOC device performance in conjunction with both photoconductive charge transport and diffractive readout models [JSEP Publs. 1, 2], the discovery and analysis of significant electric field variations within the bulk photorefractive crystal during photorefractive grating formation [JSEP Publ. 3, 4, 5] with their concomitant impact on the temporal response of the diffraction efficiency, an examination of the polarization properties of diffraction from bismuth silicon oxide under conditions of enhanced self-diffraction [JSEP Publ. 2] (which can be employed to optimize the signal-to-noise ratio of the conversion process), the development of an antireflection coating for the PICOC device fabricated from bismuth silicon oxide that is at once characterized by exceptionally low reflection coefficients and a very wide bandpass (both in wavelength and in angle of incidence) [JSEP Publs. 6, 7], an analysis and experimental implementation of the PICOC device constructed with a Stratified Volume Holographic Optical Element (SVHOE) [JSEP Publ. 8], an examination of the fundamental and technological limitations

of photorefractive grating formation as they impact current and projected PICOC device sensitivity [JSEP Publ. 9], and the development of an electrooptic technique for the measurement of the extremely high dark resistivities of as-grown photorefractive crystals [JSEP Publ. 10] (which is important for the incorporation of empirically determined parameters in theoretical models of device performance, for optimization of the crystal growth of photorefractive materials, and for the determination of the stored photorefractive grating decay time constant).

Of the many fascinating results that have emerged from these studies, perhaps the most remarkable and initially counterintuitive is the observed striking variation of the internal electric field within a bulk photorefractive material under conditions of grating recording. In these experiments, we have employed a transverse electrooptic imaging geometry as a sensitive probe of the internal electric field, as shown in Fig. 1. In this figure, the photorefractive crystal is observed from the top, with two grating writing beams incident as usual through the front surface. A third beam, of a wavelength significantly beyond the photoconductivity edge, is collimated and expanded to illuminate the crystal from the bottom, emerging from the top such that use of a polarization analyzer in conjunction with a microscope or CCTV camera provides a two-dimensional image of the local electric field distributed between the positive and negative electrodes.

Immediately following the application of a uniform electric field with the grating writing beams blocked, a uniform intensity is transmitted, indicating an isotropic field distribution within the crystal. However, after a few seconds under probe illumination only, the region near the negative electrode visibly brightens at the expense of the remainder of the bulk, and eventually multiple fringes (indicative of multiple half-wave voltages) form that are clearly visible within about 20-50 μm of the negative electrode surface.

The behavior of the internal electric field following application of the grating recording beams is even more unusual. Plotted in Fig. 2 is the temporal evolution of the bulk space charge field in a single crystal of bismuth silicon oxide under conditions of photorefractive grating formation. Initially, application of only the applied voltage produces a rapid initial rise of the field in the bulk, followed by the characteristic decline under probe beam illumination. Application of the grating recording beams is seen to

result in a dramatic drop in the bulk field (in some cases to only 5-10% of the initial field value), followed by a long slow rise in the bulk field with a time constant of order 10 sec (with grating recording beam intensities equal to 1 mW/cm^2). Simultaneous measurement of the rise time of the diffraction efficiency has also been performed by utilizing a fourth beam, as shown schematically in Fig. 1. The temporal evolution of the diffraction efficiency as shown in Fig. 2 is seen to parallel that of the bulk electric field, in complete contradiction to commonly assumed theoretical models of grating formation, and to empirical photorefractive parametrization studies.

One contributing factor to the physical origin of these unusual and striking effects is the existence of an "optical null" region near the electrodes, induced by the 180 degree phase change upon reflection characteristic of total internal reflection (a condition that applies equally well to the probe beam(s) and to the grating recording beams at typical incidence angles for photorefractive grating formation). A second factor is the presence of a blocking contact that inhibits electron injection into the crystal even in the presence of bulk photoconductive charge displacements. A complete model of the set of observed effects, including the effects of the electrodes themselves and the onset of the Schottky barrier tunneling condition, has been proposed [JSEP Publ. 3]. Further details of this model will be published shortly [JSEP Publ. 5].

These results have a clear impact on the understanding and optimization not only of PICOC devices, but also on all volume holographic optical elements based on photorefractive materials, particularly when such materials are operated in the drift rather than the diffusion mode for enhancement of either rise/fall times or saturation diffraction efficiencies.

In particular, it is of considerable interest to utilize our newfound understanding of the origins of the effect to eliminate it altogether, which will provide significant enhancements in both the expected time constants and in the overall device diffraction efficiency (which is in turn related to the device sensitivity). To this end, we have recently performed an intriguing experiment as shown in Fig. 3 in which a fifth optical beam is caused to be normally incident on the negative electrode, at a wavelength chosen to be strongly absorbed in the immediate proximity of the electrode. This beam causes strong photogeneration within the region of the

optical null, negating its effects. The modification of the field collapse is shown in Fig. 4, which depicts the probe beam intensity (a measure of the internal electric field strength) first under probe beam illumination only, then with application of the beam illuminating the negative electrode, and finally after illumination by a normally incident beam at the wavelength used for photorefractive recording. Elimination of the field drop in the bulk is observed as seen in the figure, as well as a strong reduction in the time constant for grating formation under certain conditions. Additional characterization experiments along these lines are in progress.

In an alternative approach to the development of spatial light modulators, we have begun to investigate the optimum utilization of both hybrid and monolithically integrated photonic and electronic components to optimize the performance characteristics of a broad range of spatial light modulation functions, for application to optical information processing and computing tasks. The goal of this research effort is to identify the flexibility of functionality that can be accommodated within the basic transformation required of an optically (or even electrically) addressed spatial light modulator: photodetection => functional implementation => modulation. In the implementation of such functionality, whether it be the linearization of the overall transfer characteristic or the incorporation of a threshold function, it is of considerable importance to identify those basic control elements that can best be included by means of electronic circuitry, impedance matched to both detector and modulator, and designed to occupy a minimum of the real estate assigned to the detection and/or modulation functions. Such an approach relieves a considerable burden on the photonic components themselves, in that considerable latitude in performance characteristics can be compensated for within the associated circuit design. This consideration is in turn essential for the determination of the eventual hybrid or monolithic integrability of a given device design.

For example, we have recently proposed a neural net architecture utilizing a novel strategy for the incorporation of incoherent/coherent holographic interconnections [JSEP Publs. 11, 12, 13, 14, 15]. In this architecture, the detection, amplification, functional implementation, and modulation functions required in both the neuron output and input planes are envisioned to be incorporated in two-dimensional spatial light modulators. A dual channel differential approach has been the focus of our current

designs as it inherently incorporates considerable functional generality, with capacity to accommodate both bipolar inputs and bipolar outputs. This requires the hybrid or monolithic integration of two detectors, appropriate amplification and control circuitry, and two modulators within each SLM pixel. A primary goal is to develop analog circuitry that is process compatible with both detector and modulator requirements, and at the same time utilizes minimum real estate.

Although we anticipate parallel development of monolithically integrated chips in the compound semiconductor system utilizing coupled double quantum well modulation and detection elements in conjunction with MESFETs, MISFETs, HEMTs, or RTDs (resonant tunnel diodes), the first generation chips have been designed within the silicon repertoire (MOSIS) in order to establish functional integrity, the potential for hybrid integration, and preliminary estimates of non-ideality and process-induced variances. The current chip set contains 100 x 100 μm pixels, within which 2500 μm^2 is dedicated to dual channel CMOS circuitry (see Fig. 5) that implements a differential linear transfer characteristic with both upper and lower level saturation as shown in Fig. 6 [JSEP Publs. 12, 14, 15]. Such a dual channel differential approach was intentionally chosen as illustrative of a fairly complex neuron unit design; many currently envisioned neural network models require significantly less capability within each neuron unit. And yet, our current design incorporates only fifteen transistors per pixel within 2 μm minimum feature size design rules, and allows for in excess of 10^4 dual channel pixels per cm^2.

PUBLICATIONS

1. J. Yu, D. Psaltis, A. Marrakchi, A. R. Tanguay, Jr., and R. V. Johnson, "Photorefractive Incoherent-to-Coherent Optical Conversion", in Photorefractive Materials and Applications, J. P. Huignard and P. Gunter, Eds., Springer-Verlag, New York, (1989).

2. A. Marrakchi, R. V. Johnson, and A. R. Tanguay, Jr., "Polarization Properties of Enhanced Self-Diffraction in Sillenite Crystals", IEEE J. Quant. Electron., QE-23, 2142-2151, (1987).

3. E. J. Herbulock, R. V. Johnson, and A. R. Tanguay, Jr., "Electric Field Profile Effects on Photorefractive Grating Formation in Bismuth Silicon Oxide", 1988 Annual Meeting of the Optical Society of America, Santa Clara, California, (1988).

4. A. R. Tanguay, Jr., "Device Development for Optical Computing", Conference on Lasers and Electro-Optics (CLEO '89), Baltimore, Maryland, (1989); (Invited Paper).

5. E. J. Herbulock, R. V. Johnson, and A. R. Tanguay, Jr., "Electric Field Profile Effects on Photorefractive Grating Formation in Bismuth Silicon Oxide", in preparation for Applied Physics Letters, (1990).

6. Z. Karim, M. H. Garrett, and A. R. Tanguay, Jr., "A Bandpass AR Coating Design for Bismuth Silicon Oxide", 1988 Annual Meeting of the Optical Society of America, Santa Clara, California, (1988).

7. Z. Karim, C. Kyriakakis, and A. R. Tanguay, Jr., "Improved Two Beam Coupling Gain and Diffraction Efficiency in a Bismuth Silicon Oxide Crystal Using a Bandpass AR Coating", 1989 Annual Meeting of the Optical Society of America, Orlando, Florida, (1988).

8. R. V. Johnson and A. R. Tanguay, Jr., "Stratified Volume Holographic Optical Elements", Opt. Lett., 13(3), 189-191, (1988).

9. R. V. Johnson and A. R. Tanguay, Jr., "Fundamental Physical Limitations of the Photorefractive Grating Recording Sensitivity", in Optical Processing and Computing H. Arsenault and T. Szoplik, Eds., Academic Press, New York, (1989).

10. D. A. Seery, M. H. Garrett, and A. R. Tanguay, Jr., "Electrooptic Measurement of the Volume Resistivity of Bismuth Silicon Oxide ($Bi_{12}SiO_{20}$)", J. Cryst. Growth, 85, 282-289, (1987).

11. B. K. Jenkins, G. C. Petrisor, S. Piazzolla, P. Asthana, and A. R. Tanguay, Jr., "Photonic Architecture for Neural Nets Using Incoherent/Coherent Holographic Interconnections", Proc. Intl. Conf. Opt. Comp. (OC '90), Kobe, Japan, (1990).

12. P. Asthana, H. Chin, G. Nordin, A. R. Tanguay, Jr., S. Piazzolla, B. K. Jenkins, and A. Madhukar, "Photonic Components for Neural Net Implementations Using Incoherent/Coherent Holographic Interconnections", Proc. Intl. Conf. Opt. Comp. (OC '90), Kobe, Japan, (1990).

13. B. K. Jenkins, G. C. Petrisor, S. Piazzolla, P. Asthana, and A. R. Tanguay, Jr., "Photonic Architecture for Neural Nets Using Incoherent/Coherent Holographic Interconnections", 1990 Annual Meeting of the Optical Society of America, Boston, Massachusetts, (1990).

14. P. Asthana, H. Chin, G. Nordin, A. R. Tanguay, Jr., G. Petrisor, B. K. Jenkins, and A. Madhukar, "Photonic Components for Neural Net Implementations Using Incoherent/Coherent Holographic Interconnections", 1990 Annual Meeting of the Optical Society of America, Boston, Massachusetts, (1990).

15. B. K. Jenkins and A. R. Tanguay, Jr., "Photonic Implementations of Neural Networks", Chapter 15 in Neural Networks and Fuzzy Systems: *A Dynamical Approach to Machine Intelligence*, B. Kosko, Ed., Prentice-Hall, Englewood Cliffs, New Jersey, 1991), (in press).

II. Related Publications

1. C. Kyriakakis, Z. Karim, J. J. Jung, A. R. Tanguay, Jr., and A. Madhukar, "Fundamental and Technological Limitations of Asymmetric Cavity MQW InGaAs/GaAs Spatial Light Modulators", Optical Society of America Topical Conference on Spatial Light Modulators, Incline Village, Nevada, (1990).

2. Z. Karim and A. R. Tanguay, Jr., "Bandpass AR Coating for the Photorefractive Materials $LiNbO_3$, $BaTiO_3$, CdTe, and PLZT", 1990 Annual Meeting of the Optical Society of America, Boston, Massachusetts, (1990).

3. C. Kyriakakis, P. Asthana, Z. Karim, G. Nordin, J. Rilum, and A. R. Tanguay, Jr., "Fundamental Physical and Technological Constraints on Optical Information Processing and Computing",

1990 Annual Meeting of the Optical Society of America, Boston, Massachusetts, (1990), (Invited Paper).

4. C. Kyriakakis, P. Asthana, R. V. Johnson, and A. R. Tanguay, Jr., "Spatial Light Modulators: Fundamental and Technological Issues", Optical Society of America Topical Conference on Spatial Light Modulators, Incline Village, Nevada, (1988), (Invited Paper).

5. A. R. Tanguay, Jr., "Physical and Technological Limitations of Optical Information Processing and Computing" Materials Research Society Bulletin, Special Issue on Photonic Materials, XIII(8), 36-40, (1988); (Invited Paper).

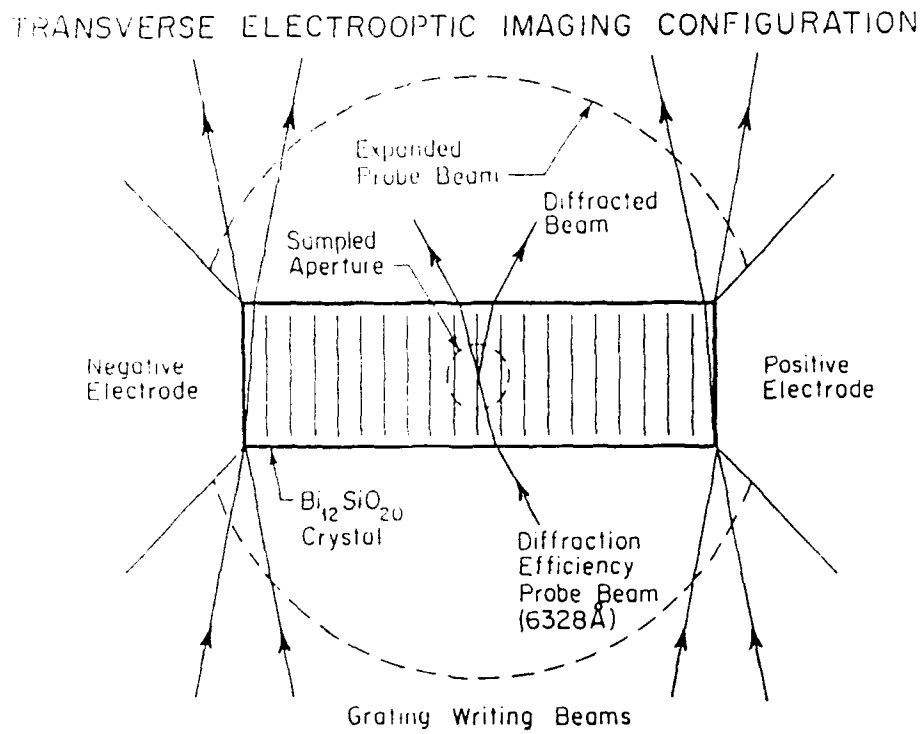

Fig. 1. Schematic diagram of the transverse electrooptic imaging configuration utilized to determine the effects of applied bias, probe beams, and grating recording beams on the internal electric field in a single crystal sample of bismuth silicon oxide ($Bi_{12}SiO_{20}$).

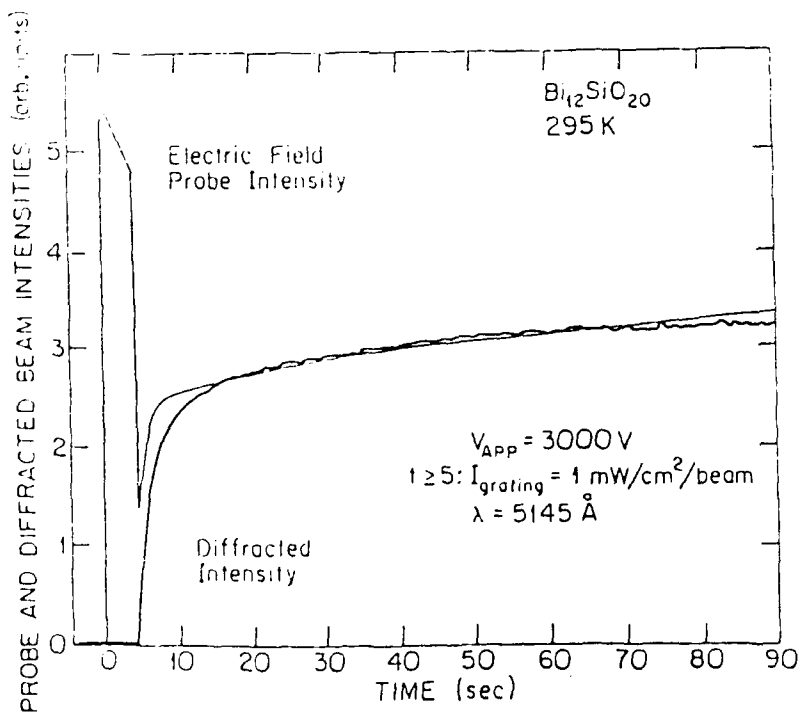

Fig. 2. Temporal evolution of the bulk space-charge field and diffraction efficiency in a single crystal of bismuth silicon oxide under conditions of photorefractive grating formation.

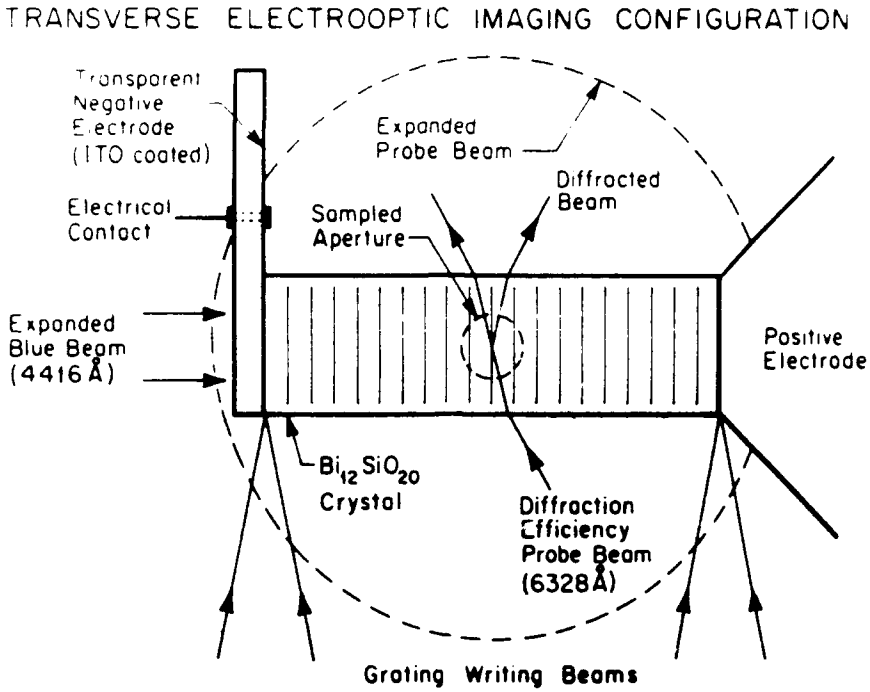

Fig. 3. Schematic diagram of the transverse electrooptic imaging configuration modified to include a transparent contact at the negative electrode for incorporation of a fifth input beam.

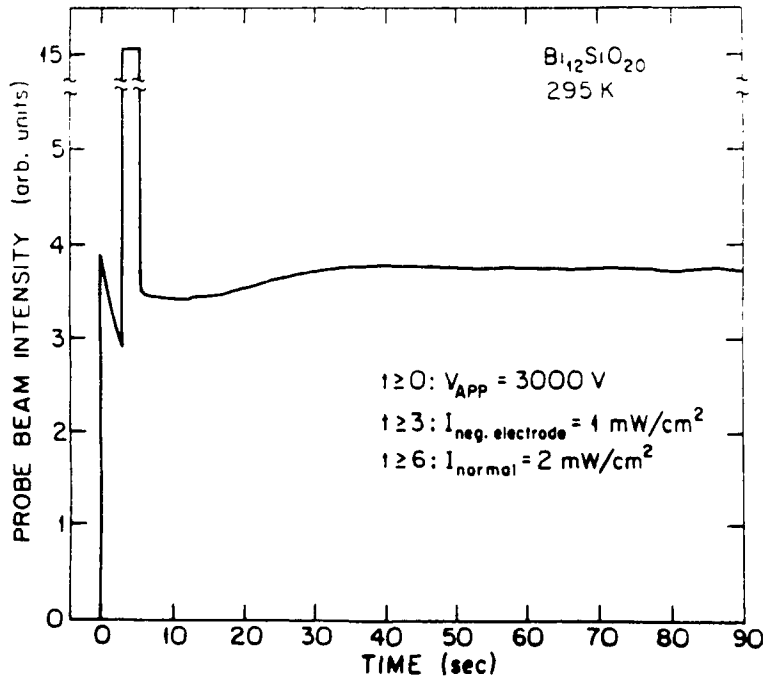

Fig. 4 Plot of the probe beam intensity as a function of time following application of the probe beam (t = 0), the beam transmitted through the negative electrode (t = 3), and a uniform beam normally incident to the front face of the single crystal sample of bismuth silicon oxide ($Bi_{12}SiO_{20}$) (t = 6).

Fig. 5. Schematic diagram of a dual channel CMOS differential amplifier, with provision for dual photodetector inputs as well as dual modulator element outputs. Provision is made for an external (electrically or optically) bias voltage for incorporation of a level offset function.

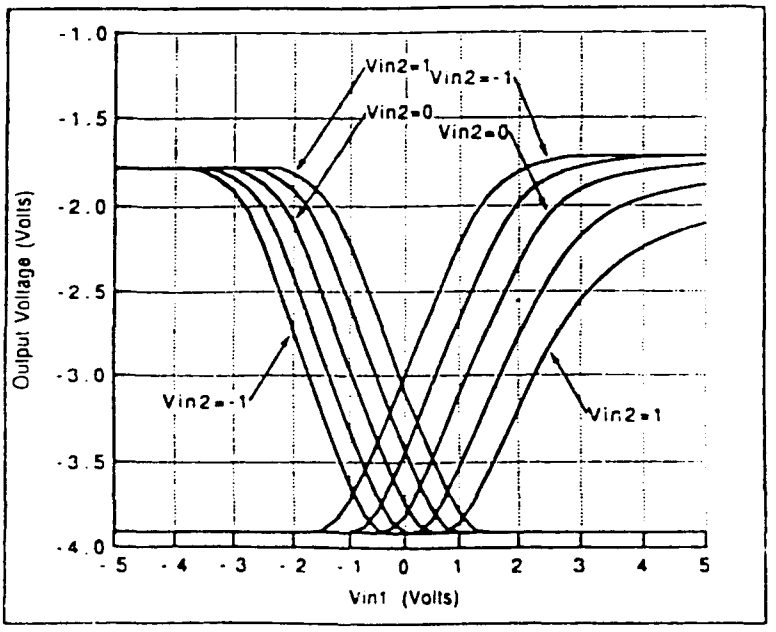

Fig. 6. Output transfer characteristic curves for both outputs of a dual channel CMOS differential amplifier, with 15 transistors incorporated in an area of 2500 μm^2 (25 x 100 μm).

Optoelectronic and Quantum Structures Using Pristine and Irradiated Organic Compounds

S. R. Forrest
SS3-4

PROGRESS

During the last few years, considerable progress has been made in our laboratory in fabricating and understanding heterojunctions based on crystalline organic (CO) semiconductors. In particular, considerable concentration of our effort has been devoted to the improving the growth process of such materials as 3,4,9,10 perylenetetracarboxylic dianhydride (PTCDA) which has exhibited extremely high quality optical and electronic properties. As a result of our investigations regarding growth, we have found a means of routinely depositing single crystalline films of CO materials on substrates such as glass or inorganic semiconductors such as InP and Si. Hence, fully organic MQW structures, and high mobility photodetectors have all been realized for the first time using these interesting, and useful organic compounds. Much of our fundamental understanding of these materials leading to the rapid realization of high quality optical and electronic devices was gained using JSEP support. Below is a list of publications which directly acknowledge this support. We briefly summarize here the highlights of our JSEP research during the 1990:

Low loss waveguiding of several TE modes coupled into PTCDA slab and rib waveguides was demonstrated using, end-fire, prism and grating coupling techniques. The very low losses encountered (relative to other results for CO materials) are due, in part, to the extremely high degree of crystalline ordering and purity of the films grown at low substrate temperatures (90 K) using organic molecular beam deposition -- a technique pioneered in our laboratory at USC. Briefly, the waveguides were fabricated by depositing the thin films at a rate of 1 - 5 Å/s onto the cold substrates, to a thickness of approximately 1 μm. We find that, under these conditions, the entire film is single crystalline, and hence scattering losses from grain boundaries in polycrystalline films is reduced to zero.

The rib waveguides were fabricated as follows: A 2 - 10 μm wide strip of photoresist was patterned after it was deposited onto

an InP substrate at a thickness of 5000Å. Next, PTCDA was deposited onto the wafer surface. Due to the relatively low index of refraction of the photoresist (n = 1.6), the PTCDA deposited on this strip formed the waveguide, whereas PTCDA deposited directly on the InP (with n =3.4) did not guide. The wafer was then cleaved perpendicular to the strips such that sharp end faces to the guides were formed. Guides as thin as 2 μm were achieved using this process. Typical guide lengths were 1 - 1.5 cm. A schematic view of the waveguide is shown in Fig. 1.

As a result of the high degree of crystalline ordering of the PTCDA deposited by organic molecular beam deposition, total guide losses of < 2.5 dB/cm were obtained. To our knowledge, this is by far the lowest loss ever achieved using CO materials. It is a particularly exciting result given the fact that the materials employed in the waveguiding also have excellent electronic properties which we have demonstrated in past work. Hence, we now have a novel and very versatile materials technology which can be employed in a wide variety of optoelectronic integrated device applications.

Next, the index of refraction of the guided modes was measured using standard coupled mode theory for waveguides. Here, we find the index for TE modes launched along the in-plane projection of the optical c axis was $n_{TE} = 2.017$ at λ = 1.06 and 1.3 μm. However, we were unable to launch TM modes into any waveguide, whether slab or rib, or whether the guide was formed on glass or photoresist. Indeed, after 1 mm of guide, the TE/TM mode intensity ratio was > 50 dB indicating complete attenuation of the TM modes over very short propagation distances. Furthermore, in launching either polarization, we were unable to detect any TM mode intensity at the output of the guide.

Recent measurements of the index perpendicular to the waveguide indicates that n_{TM} = 1.35 in this direction, giving Δn = 0.65 in the vertical vs. the horizontal directions. Since n_{TM} is so small, PTCDA does not guide these modes when deposited on glass (with n = 1.45) or photoresist.

The very large asymmetry in n in our thin films is indicative of the nearly perfect ordering achieved in the growth process. Fundamentally, this degree of index difference is expected for a molecule such as PTCDA if the electron orbital π-system is

completely delocallized across the planar surface of the molecule. Then the dielectric constant perpendicular to the molecular stacking direction is determined by the dipole moment in that direction, which is proportional to the length of the molecule (approximately 10 Å). This is in contrast to the dielectric constant parallel to the stacks, where we expect the dipole moment is proportional to the intermolecular stacking distance (3.21 Å). Such an asymmetry in the dielectric constant leads immediately to an index asymmetry of the same magnitude as that observed. Note, therefore, that to observe this index difference, we infer that the molecular stacks contain few defects, and that the crystalline order is nearly perfect over large distances covered by the waveguides.

In summary, JSEP has played a central role this year in our achieving highly ordered optical structures such as waveguides fabricated using OMBD-deposited PTCDA. It has been instrumental in leading to several breakthroughs which puts the technology on the brink of demonstrating complex, and novel optoelectronic integrated circuits which utilize the most advantageous features of both organic and inorganic semiconductors. The compatibility of these two materials systems allows for an enormous range of flexibility in device design and functionality which, to date, has been completely inaccessible to devices made only from inorganic materials.

PUBLICATIONS

1. "Optical waveguides in crystalline organic semiconductor thin films", D. Y. Zang, Y. Q. Shi, F. F. So, S. R. Forrest and W. H. Steier, accepted, Appl. Phys. Lett. (Feb. 11, 1990).

2. "Crystalline organic semiconductor thin film optical waveguides", D. Y. Zang, Y. Q. Shi, F. F. So, S. R. Forrest and W. H. Steier, Opt. Soc. Am. Annual Meeting, Boston, MA (Nov., 1990).

3. "Growth and characterization of organic semiconductor heterojunctions and multiple quantum wells", F. F. So, L. Y. Leu and S. R. Forrest, SPIE Symposium on Superlattices and High T_C Superconductors, **1285**, 51 (1990).

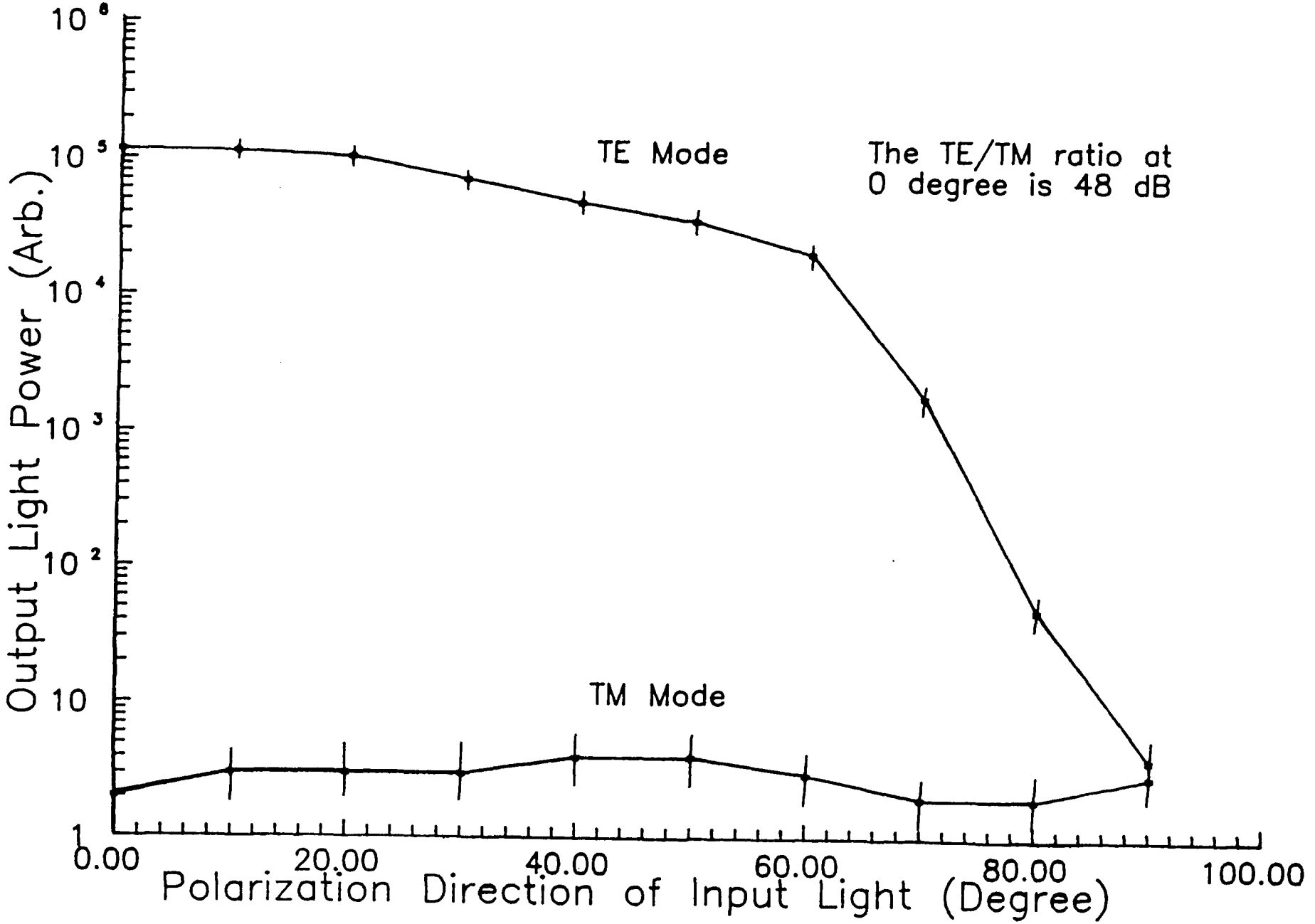
Output Light Power (Arb.)
10 6
10 5
10 4
10 3
10 2
10
1
TE Mode
The TE/TM ratio at
0 degree is 48 dB
TM Mode
0.00
20.00
40.00
60.00
80.00
100.00
Polarization Direction of Input Light (Degree)

FIGURE II

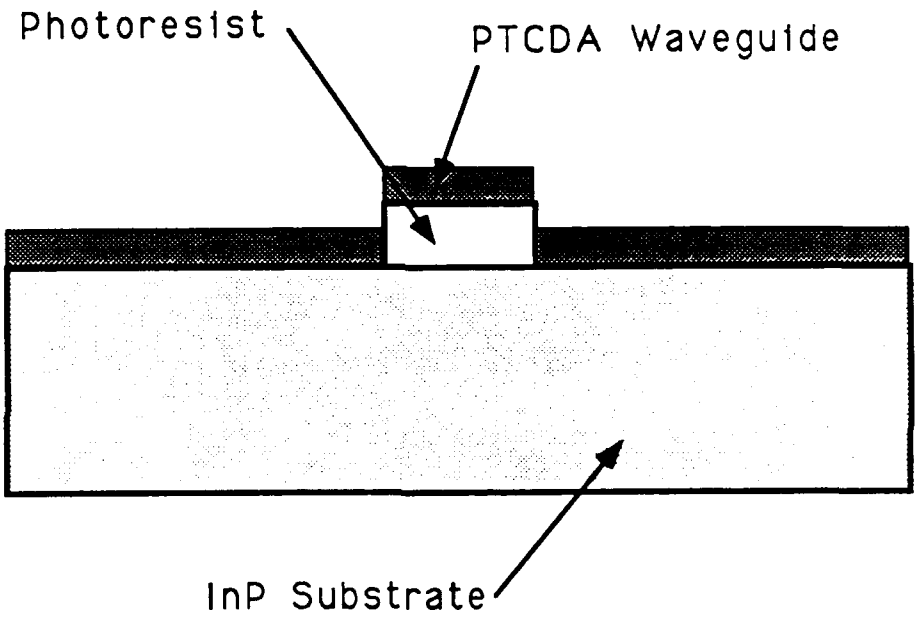

FIGURE I

Research to Improve Long Wavelength Infrared Semiconductor Lasers

E. Garmire
QE3-1

Progress

During the past year we have completed an investigation of the temperature dependence of InAs double heterostructure lasers. We have taken the approach of performing a theoretical analysis and modelling, using the best values we could find in the literature for all the parameters which the calculation required. InAs lasers fabricated to date have not operated at higher than 150 K. It was thought that Auger recombination was the limiting mechanism. We have shown that carrier leakage due to drift current is in fact larger than Auger recombination, in experimental InAs lasers, which use InAsPSb cladding regions containing 25% P. Operation at higher temperatures will not be possible with such structures, due to carrier leakage. The result of this analysis is shown in Figure 1a. The good agreement with our predicted thresholds and Horokoshi's experimental data indicate the correctness of our model.

We have studied the liquid phase epitaxial growth properties of InAsPSb alloys lattice-matched to InAs and determined that the highest reasonable phosphorus content (grown at 600 C) would be 46%, which would offer more carrier confinement than Horokoshi's structure. We have modelled this structure and optimized the active layer thickness. The result, shown in Figure 1b, shows clearly that carrier leakage is no longer a problem until very near room temperature. Operation at 200 K or above is now feasible.

If phosphorous is increased further, by using MOCVD or CBE as a fabrication technique, further reduction in threshold comes, not only from reducing carrier leakage, but also from improving optical confinement. With the limiting composition of InP0.69Sb0.31, the temperature at which thresholds as low as 10 kA/cm2 can be acnieved is increased to 220 K, as shown in Fig. 1c. Finally, by using AlAs0.16Sb0.84 as a cladding layer, the temperature can be increased to 250 K, as shown in fig. 1d.

In order to perform these calculations it was necessary to know the band offset between several III-V alloy compounds. We did this by creating an empirical rule to predict relative valence band positions, extrapolating

from III-V binary compounds using Vegard's law. We calculated these III-V binary band offsets using ternary and/or quaternary alloys which have been previously measured by the capacitance-voltage profiling technique. The results of this study are shown in the Table and compared to the work of other authors.

The outcome of this year's study is the decision that the suitable long wavelength lasers cannot be made with LPE, but require chemical beam epitaxy fabrication techniques. We have predicted that the lowest threshold devices will use AlAsSb cladding layers and should be able to operate near room temperature. The limiting factor with this geometry is Auger recombination. Further reduction of threshold may be possible using multiple quantum wells, which raises the gain and should reduce the required carrier densities, reducing Auger recombination. Alternatively, strained layer devices may have reduced Auger recombination. In is interesting to note that this cladding forms a heterostructure with InAs for which we predict essentially no valence band offset. However, our model shows that electron and optical confinement is sufficiently large that hole leakage is not a problem.

PUBLICATIONS

1. Y. Tsou, A. Ichii, E. Garmire, "Temperature Dependence of InAs DH Lasers" submitted to J. Appl. Phys.

2. A. Ichii, Y. Tsou, E. Garmire, "An empirical rule of band offset between III-V aloy compounds" submitted to J. Appl. Phys.

3. N. M. Jokerst, E. Garmire, "Sensitive Band-filling nonlinearities using selective carrier confinement" submitted to Electronics Letters

4. E. Garmire "Semiconductor Nonlinearities enhanced by Carrier Transport" (Invited) International Congress on Optical Science and Engineering, The Hague, March, 1990

5. E. Garmire "Prospectives for Long Wavelength Lasers" Invited lecture at Telebras, Campinas, Brazil, August, 1990

6. E. Garmire, "Optical nonlinearities enhanced by carrier transport" in "Laser Optics of Condensed Matter, vol. 2, edited by Alex Maradudin, published by Plenum Press, 1990

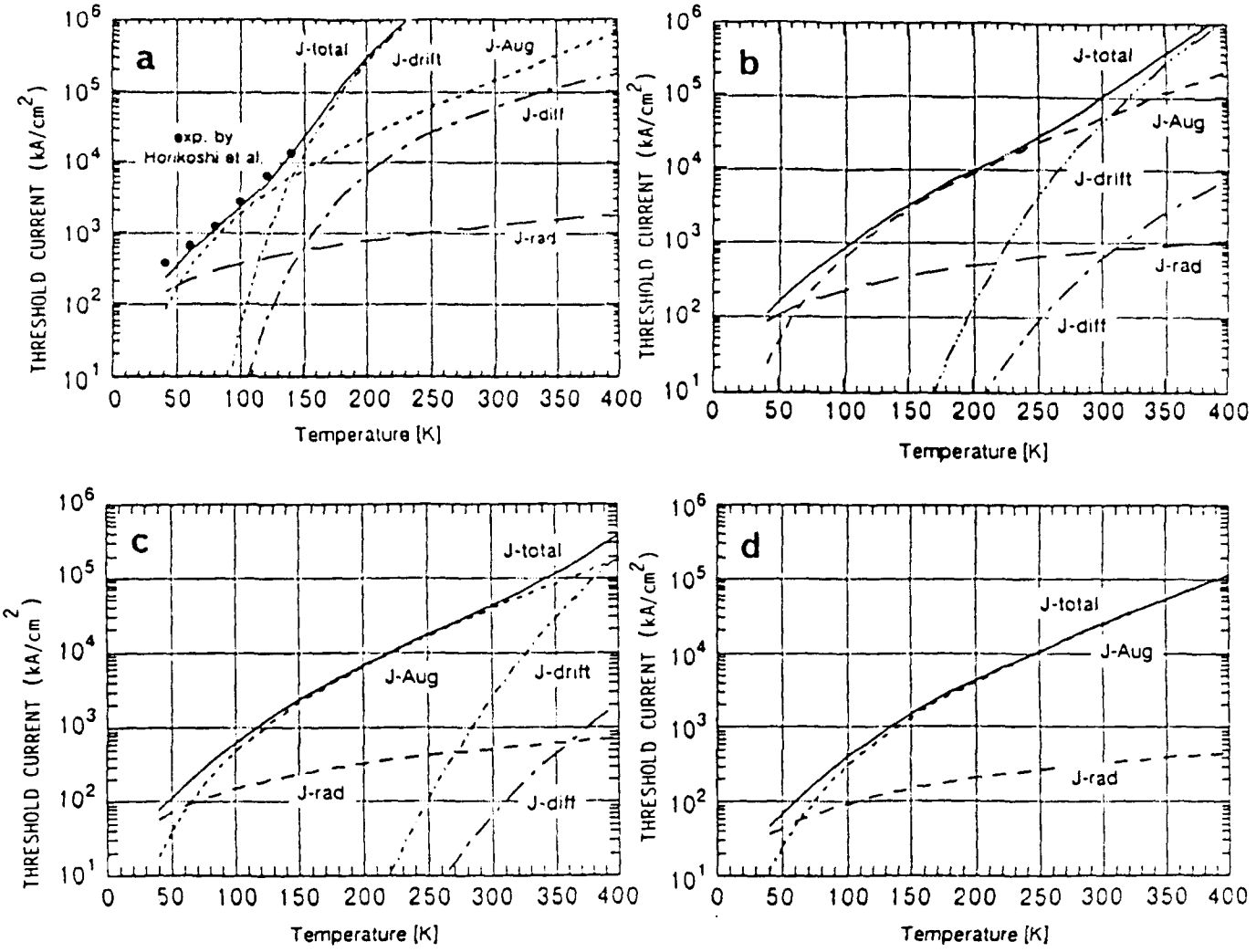

Figure 1. Temperature dependence of threshold current density of InAs lasers with different claddings: a) InAsPSb (25% P); b) InAsPSb (46% P); c) InPSb; d) AlAsSb.

Table 1 POSITIONS OF THE VALENCE BAND EDGES OF III-V BINARY COMPOUNDS RELATIVE TO AlAs (eV)

Material	This Work	Tersoff	Harrison	Katnani	Schuermeyer
AlP	-0.48	-0.22	-0.46	---	---
AlAs	0	0	0	0	0
AlSb	0.76	0.60	0.90	---	0.90
GaP	0.24	0.24	-0.43	-0.36	---
GaAs	0.48	0.55	0.04	0.27	0.40
GaSb	1.16	0.98	0.88	0.39	1.30
InP	0.20	0.29	-0.07	-0.09	---
InAs	0.65	0.55	0.36	0.27	0.80
InSb	---	1.04	1.16	0.49	---

A Sprectroscopic Study of Basic Processes in Electrically Exicited Materials

M. A. Gundersen
QE3-2

PROGRESS

III-V Static Induction Transistor/thyristor

Fabrication of the recessed-gate, GaAs "Static Induction Transistor" is reaching its final stage. The channel region ($N_D=2x10^{14}$ cm^{-3}, 45 mms) and the n^+ source region ($N_D>10^{18}$ cm^{-3}, 2.5 mms) were grown atop a 450 mm, n^+ GaAs substrate by vapor-phase epitaxy. Following conventional degreasing techniques, the wafers were initially subjected to a $H_2SO_4:H_2O_2:H_2O$ (5:1:1) treatment, and then a thin oxide layer was grown by immersion in warm (T=70 C) deionized water. The oxide was removed by $HCl:H_2O$, and after rinsing with methanol, the wafers were quickly transferred to the reactor and 900 A of SiN was deposited to serve as the surface passivant. SiN is hygroscopic and is an excellent barrier to alkali ion migration. The nitride layer was then patterned and reactive ion etching was performed to open windows for the recessed-gate etch. The recessed-gate etch was performed using an isotropic, diffusion-limited etch ($HCl:H_2O_2:H_2O$ (40:4:1)). The nitride layer was then removed and Be ion implantation was performed through a patterned photoresist mask to form the p^+ gate regions. Upon deposition of a nitride coating, the wafers were annealed at 700 C for 20 minutes in a nitrogen ambient. Next, the nitride was stripped and 1000 A of new nitride was re-deposited. Following this step, RIE was implemented to open up gate and source contact windows for metallization. The final step in the processing of the device, namely gate, source and drain metallization using lift-off techniques, will be completed in the very near future. Upon completion, extensive DC and pulsed optoelectronic testing will be performed utilizing low energy (1-2 mJ) solid state laser arrays as the optical source. Test facilities for such measurements have been designed and completed.

LPE System for High Power Devices

The design and testing of the vertical liquid phase epitaxial system has been completed. Growth was initially performed on semi-insulating (EL2 doped) GaAs substrates. Tapered layer thicknesses of up to 20 mms were achieved, however the surface morphology was poor. It is believed that the tensile forces at the Ga melt surface were not adequate for proper wipe-off of the excess liquid from the surface of the wafer, and thus mirror finish surfaces could not be obtained. Currently, effort is under way to transform the system into a horizontal growth reactor. The advantage of horizontal growth reactors lies in the fact that provisions for mechanical wipe-off of the excess Ga from the wafer surface upon completion of the layer growth can be incorporated in the reactor. In this case, a high purity graphite boat and slider assembly are utilized. The design and fabrication of the graphite boat and slider has been completed. Upon modification of the existing high purity quartz reactor tube, growth of thick (>20 mms), high purity, undoped ($N_D<10^{15}$ cm^{-3}) GaAs layers will be continued.

Research is also under way to study new Schottky / ohmic metal systems on n-GaAs which are inherently stable at high temperatures (500 C). At this stage, tungsten is the only single element metal which results in rectifying junctions on n-GaAs and which is metallurgically stable at high temperatures (<600 C). Unfortunately, due to the large mismatch in the thermal expansion coefficients, thick (>2000 A) tungsten layers tend to peel-off GaAs, while thin layers result in large values of spreading resistance. A new compound metallic system (Co_xGa_{1-x}) is currently under study. Preliminary experiments have indicated that the Co_xGa_{1-x} / n-GaAs system is stable at temperatures reaching 500 C, with no long order interdiffusion observed. Our goal is to study this new system towards applications in high power devices, since contact failure is a major mechanism for device degradation under such operating conditions. These studies will be completed in the next few months.

III-V Opto-Thyristors

GaAs based opto-thyristors were fabricated with Cr doped semi-insulating base layer, and displayed desirable switching characteristics. The junctions were formed with metal-organic chemical vapor deposition (MOCVD). The DC blocking voltages of the opto-thyristors were >800 volts, and the peak pulsed currents were ~300 A. The current rates of rise were $>10^{10}$ A/sec, which were limited by the external circuit.

It was found that an effect called "lock-on" effect plays a dominant role during the conduction phase. This effect is currently being studied experimentally and theoretically. Presently, this effect is understood as an interaction of the deep-level trapping/recombination and the formation of domains due to the electron-transferred effect. Others have suggested double injection as the major mechanism. More experiments and theoretical works are needed.

A new design for III-V compound based opto-thyristors is being pursued — a heterostructure opto-thyristor (HOT). This design takes advantage of the advanced state of the GaAs-AlGaAs heterojunctions. The use of heterostructure allows a high gating efficiency and consequently, a fast current rate of rise. The device is fabricated with vapor phase epitaxy and MOCVD.

Recent results include:

- Very promising experimental GaAs thyristor results
- Development of growth methodology *and* facility
- High voltage modeling developed, accepted for publication

These demonstrate very significant progress in understanding the physics that limit development of solid state switches for pulsed power applications. In addition, the work was actually demonstrated by optically triggered thyristor switching, and thus has made real progress towards implementation of the physics and

development of pulsed power switches. Such switches will have applications for light weight, high power airborne and other applications - such as laser and accelerator pulsed power modulator components.

Publications

1. "An optically gated, glow switch Marx bank," R. Liou, H. Figueroa, Y. Hsu, G. Kirkman, and M. A. Gundersen, accepted for publication in IEEE Trans. Elec. Devices.

2. "Avalanche breakdown in p-n AlGaAs/GaAs heterojunctions," J. H. Hur, C. W. Myles and M. A. Gundersen, J. Appl. Phys. **67** (11), 1 (1990).

3. "GaAs based opto-thyristor for pulsed power applications," J. H. Hur, P. Hadizad, S. G. Hummel, K. M. Dzurko, P. D Dapkus, M. A. Gundersen and H. R. Fetterman, IEEE Trans. on Elec. Dev., accepted for publication.

4. "Lock-on effect in pulsed semiconductor switches," M. A. Gundersen, J. H. Hur, H. Zhao and C. W. Myles, submitted to Appl. Phys. Lett.

Nonlinear Optical Waveguiding in Compound Semiconductors

William H. Steier
QE3-3

PROGRESS

High Contrast Photo-induced Birefringence Modulator - High contrast or high on-off ratios in opto-optical switches is desirable for high signal to noise ratios in switching matrices and is required for optical computing architectures which use large fan-ins for the next layer of devices. We have completed an analysis and experimental study of a device which uses polarizers and optically stimulated electrobirefringence in quantum well waveguides to achieve a high contrast ratio in the signal beam.

The waveguide, which is in the intrinsic region of the photodiode, is shown in Figure 1. It was grown by MOCVD, wet etched to form 1.5 micron ridges for lateral confinement, electrically contacted with evaporated metal, and then cleaved into 1.35 mm long waveguides. The diode dark current was measured as 42.6 nA/mm^2 with 5 volts reverse bias. The device has a responsivity of 0.272A/Watt when 790 nm light is incident from above. When 884 nm light is coupled into the waveguide, it is calculated that 75.1% of the power propagates in the MQW region, which consist of twenty five 100Å GaAs wells bounded by 100Å $Al_{0.3}Ga_{0.7}As$ barriers.

During operation, a potential of 4.2 volts was placed across the device and 33K ohm resistor connected in series as shown in Figure 1. Light at 884 nm and polarized at 45 degrees from the waveguide plane was coupled into the waveguide. The compensator was adjusted such that, together with the waveguide, they form an integer half waveplate. When the 790 nm beam strikes the device from above, photocurrent is generated and the voltage drops across resistor rather than the waveguide diode structure. As the field in the quantum well waveguide drops, the birefringence is modulated through the linear and quadratic electrooptic coefficients and the light transmitted by the analyzer changes. Contrasts as high as 200:1 have been observed. The speed is limited by the photodiode

capacitance of 271 pf/mm^2 and the load resistor. By minimizing unused photodiode area, the $R_{load}C_{diode}$ time constant is expected to be reduced to 100ns. Although the responsivity is lower at 884 nm, self switching can occur. Because of the difference in responsivity at 884 nm and 790 nm, optical gain is possible.

The properties of the photo-induced birefringence modulator are:

a. Contrast ratio (observed) 200:1
b. Throughput (observed) 40%
c. Gain, P(890)/P(790) 10
d. Switching energy per channel (extrapolated) 15pJ
e. Switching time (extrapolated) 50nsec.

Measurement of the Linear and Quadratic Electrooptic Coefficients as a Function of Wavelength - The primary effect used in most charge transport nonlinear optical effects is the electooptic effect; either the linear (Pockels) or the quadratic (Kerr) effect. These effects show dispersion near the semiconductor bandgap and it is therefore necessary to have accurate data on the value of these coefficients to determine optimum operating wavelengths for these devices. Since operation is normally in a relative high loss region of the spectrum it is necessary to set the device interaction length by balancing the effects of loss and electrooptic coefficient.

The waveguiding geometry makes a measurement of the r_{41} and the $(R_{11}-R_{12})$ coefficients possible. However it is difficult to separate out the electro-absorption effects from the electroooptic effects particularly near the bandgap; just the region where most of the interesting dispersion occurs. Using the same device structure as for the photo-induced birefringence modulator but driving the modulator with an r-f source, we have made a series of measurements of the dispersion of these coefficients. To avoid the electro-absorption effects we have devised a measurements technique which measures the ω and 2ω components of the ratio of the modulator output before and after the analyzer.

Integrated Optics Nonlinear Resonator with Distributed Coupling -Fabry-Perot resonators have been used to, in effect, enhance material nonlinear effects by increasing the optical intensity inside the resonator at the price of narrow band operation.

This approach has led to several practical nonlinear optical devices. We have recently done an analysis to demonstrate that the effective nonlinear properties can be increased still further and novel switching devices are possible using an integrated optics side-coupled resonator. In this structure, shown in Figure 2, a waveguide resonator, filled with nonlinear or electrooptic material and terminated with Bragg gratings, forms a directional coupler with an adjacent waveguide. The structure has two advantages: (i) the nonlinear phase shift per round trip within the resonator is increased due to the nonlinear effects of the reflection coefficient of the coupled waveguide and (ii) the magnitude of the coupling to the resonator is a function of the intensity inside the resonator. The device is similar in construction to the linear resonant optical reflector (ROR) used for linewidth narrowing of semiconductor lasers.

In our analysis the device exhibits bistability and optical or voltage controlled switching. We have developed a formalism for this analysis which follows that used in conventional bistability and therefore makes comparisons to conventional devices easier. It allows us to calculate the critical intensity and the critical mistuning for optimized structures. The critical intensity is the necessary incident optical intensity to just show bistable switching and the critical mistuning is a measure of the required magnitude of the change of index of refraction of the nonlinear material.

In comparing this resonator to the conventional Fabry-Perot resonator the critical parameters are the linear absorption of the material and the maximum finesse of the resonator. In any practical device the maximum finesse will be limited, in the low loss materials, by alignment and fabrication errors and not by the linear absorption coefficient. In this analysis we have therefore assumed that the finesse is limited to the range of 5 to 8; typical of a practical device.

In the distributed resonator the critical intensity can be reduced by about 25% for a finesse of 5 and linear absorption on the order of 1 cm^{-1} as compared to a Fabry-Perot. In general the advantage in critical intensity is with the distributed resonator for a finesse of less than 7 and an absorption of less than 3 cm^{-1}. The critical mistuning for the distributed resonator is always less than the Fabry-Perot by 10-20% for a finesse less than 8 and losses less than 4-5 cm^{-1}.

The three output ports and the compatibility with integrated optics technology make this a promising structure for several applications. The reduced optical intensity required for switching

can be important in systems considerations and the reduced critical mistuning and hence the reduced nonlinear index change eases material requirements.

PUBLICATIONS

1. Serge Dubovitsky and William H. Steier, "Integrated Optics Nonlinear Resonator with Distributed Coupling" Paper FJ4, Optical Society of America Meeting, Boston, Mass., Nov., 1990.

2. R. T. Sahara, W. H. Steier, S. G. Hummel, P. D. Dapkus, "High Contrast Photo-induced Birefringence Modulator", Paper OE8.1, LEOS '90, Boston, Mass., Nov. 1990.

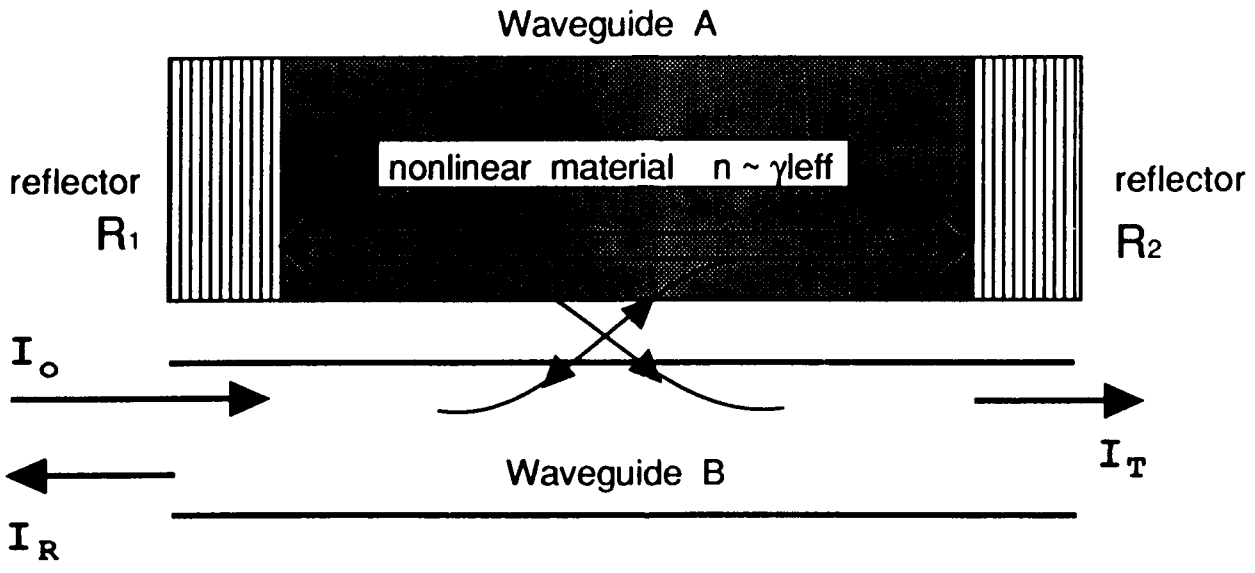

Figure 2

Nonlinear Distributedly Coupled Resonator

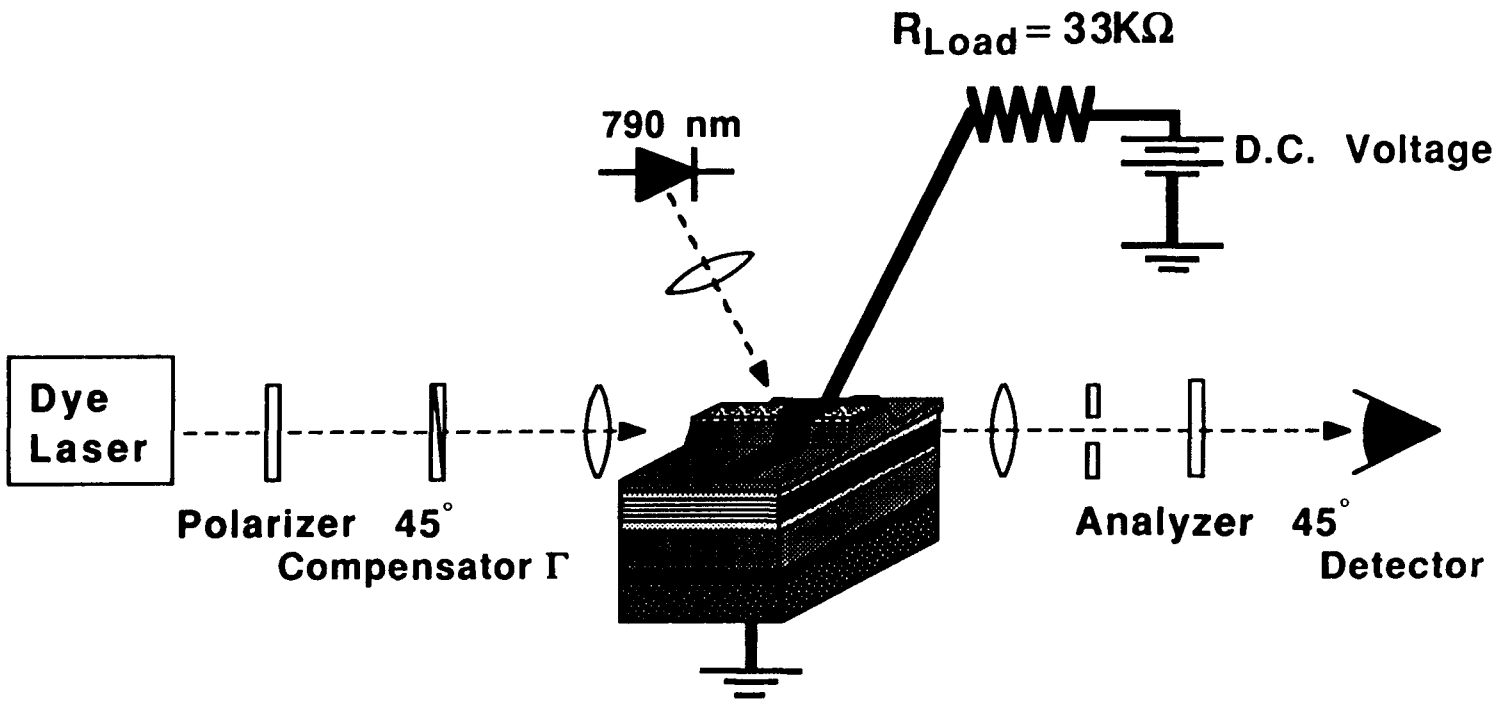

Figure 1 Photo-Induced Birefringence Modulator Experiment Schematics

Parallel Optical Processing in Photorefractive Materials

J. Feinberg
QE3-4

Progress

We have been studying the photorefractive effect and its applications. In last year's report we summarized how we solved the puzzle of the apparent sublinear dependence of photorefractive speed on intensity in $BaTiO_3$, and showed that the culprit is a level of shallow acceptors. An important result of our theory is that the assumed sublinear response function I^x is not, in fact, the correct functional dependence of the photorefractive speed on light intensity; the actual function is considerably more complicated. We performed detailed experiments to confirm our theory, and these results were published in Physical Review Letters this past year.[1] These experiments also indicated that $BaTiO_3$ crystals can be made more sensitive in the near IR by heat treating the crystals.

We have also investigated how a sequence of short laser pulses will interact in a photorefractive crystal. We derived a theory predicting how two intersecting trains of pulses, such as from a mode-locked laser, can build up a grating in a photorefractive crystal.[2] We show that this grating will couple the laser pulses and distort their shape as they traverse the crystal. This theory predicts that photorefractive crystals may be useful for customizing the temporal shapes of short laser pulses for communications applications. Examples of such pulse shaping are shown in the figure below.

One prediction of our theory is that the coupling strength of a photorefractive grating (that has been built up by two intersecting pulse trains) is proportional to correlation of the incident optical electric fields at the entrance face of the crystal. This result

implies that a photorefractive crystal can be used to measure the duration of an optical pulses, as was experimentally verified[3] by Vince Dominic, who has a JSEP sponsored fellowship. This pulse-measuring technique is especially useful for determining the temporal shape of light pulses that are too weak to be measured by the usual technique of second-harmonic generation.

PUBLICATIONS

1. D. Mahgerefteh and J. Feinberg, "Explanation of the apparent sublinear photoconductivity of photorefractive barium titanate," Physical Review Letters 64 2195 (1990).

2. X. Steve Yao, Vince Dominic, and Jack Feinberg, "Theory of beam coupling and pulse shaping of mode-locked laser pulses in a photorefractive crystal," JOSA-B December 1990.

3. Vince Dominic, X.Steve Yao, R.M. Pierce, "Measuring the coherence length of mode-locked laser pulses in real time,' Applied Physics Letters 56 521 (1990).

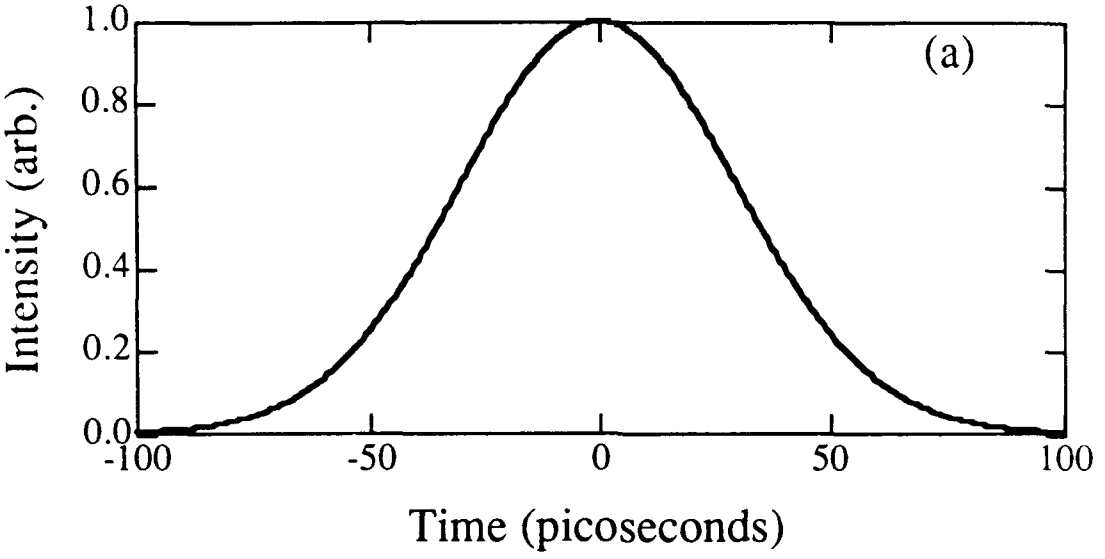

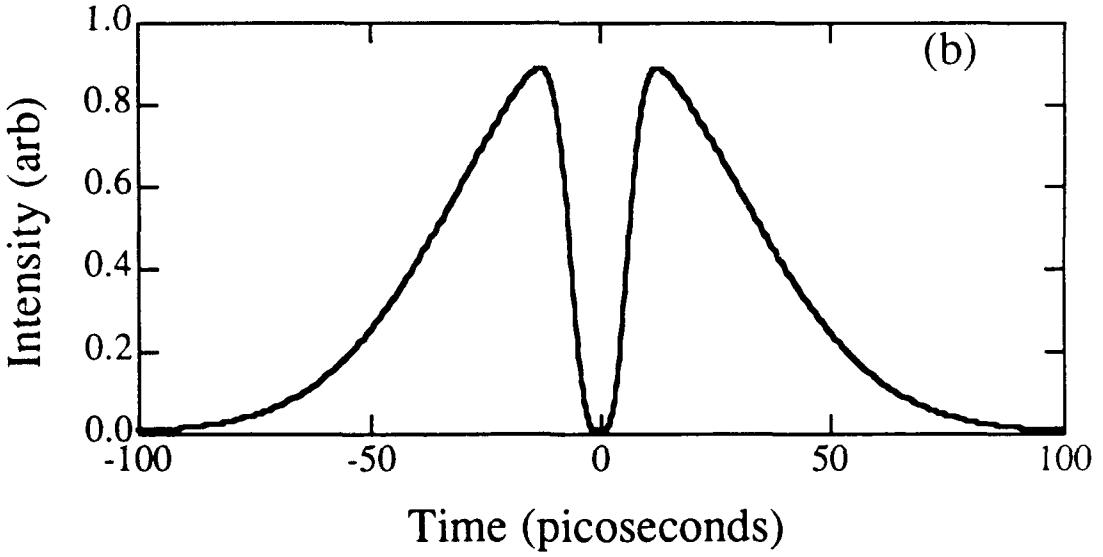

FIGURE: Calculated pulse shaping using two-beam coupling in a barium titanate crystal. The top graph shows the temporal shape of the incident Gaussian beam. The bottom graph shows the same pulse after the crystal. A sharp spike has been carved out of the pulse.

Spread Spectrum Receiver Design for Intense Jamming Environments

R. A. Scholtz
IE3-1

PROGRESS

Since our last report, we have been working on cases based on the assumption that the pre-despreading adaptive interference rejection processor can respond to the non-stationary jamming instantaneously. In analyzing such simplified cases, we may get better insight into how the time-varying S-curves and the effective noise power spectral densities of the equivalent tracking loop are related to parameters of the interference. (e.g. the peak jamming power and the duty factor of the periodic pulse jammer, etc.)

Based upon the above mentioned assumption, the equivalent code tracking loop we are studying now contains a normalized nonlinear S-curve derived from one-chip early-late loop design and the additive effective noise power spectral density switches between two levels as the jammer switches on and off. The loop filter is chosen to have a delta impulse response so that the tracking is first-order for simplicity.

The normalized tracking error, measured in chip times and modelled using equivalent code tracking loop, is a diffusion process with absorbing boundaries to be set at plus one and minus one chip time, which represent the boundaries beyond which the code tracking loop will announce an out-of-lock condition and the receiver will reinitiate the code acquisition procedure. Its drift coefficient is the negative of the normalized nonlinear S-curve and the diffusion coefficient is proportional to the reciprocal of the signal-to-interference-plus-noise ratio (SINR). The corresponding Fokker-Planck equation for the tracking error density as a function of time can be easily set up and solved numerically.

The Fokker-Planck equation with absorbing boundaries problem is

$$\frac{\partial p(e,t)}{\partial t} = \frac{\partial}{\partial e}[s(e)p(e,t)] + \frac{1}{r}\frac{\partial^2}{\partial e^2}\, p(e,t) \ ,$$

with the absorbing boundary condition $p(\pm 1,t) = 0$, where $e=(T-T')/T_C$ is the normalized tracking error, $p(e,t)$ is the density function, $s(e)$ is the normalized nonlinear S-curve, and r is the SINR. This has been solved numerically for different duty factors of the periodic pulse jammer with fixed average jamming power. (See figure 1.)

By examining the cross sections of the numerical solution at different times (see figure 2), we have found that a quasi-stationary solution, i.e., a solution in which the time dependence and the state dependence can be separated ($p(e,t)=a(e)b(t)$), apparently exists and dominates the absorption (loss of lock) transients shortly (less than one loop time constant) after the jammer switches its (on-off) state. The cross-section $a(e)$ must satisfy the equation

$$\frac{d^2}{de^2} a(e) + f(e)a(e) = \beta a(e) ,$$

where $f(e)$ is a known function of the tracking loop's normalized S-curve and the SINR, and β is an unknown. For tracking loops, the above equation presents a self-adjoint boundary value (Sturm-Liouville) problem. When $f(e)$ is a constant, then this equation can be solved analytically with the boundary conditions $a(\pm 1)=0$, but we have not yet found solutions for the functions $f(e)$ that are of interest.

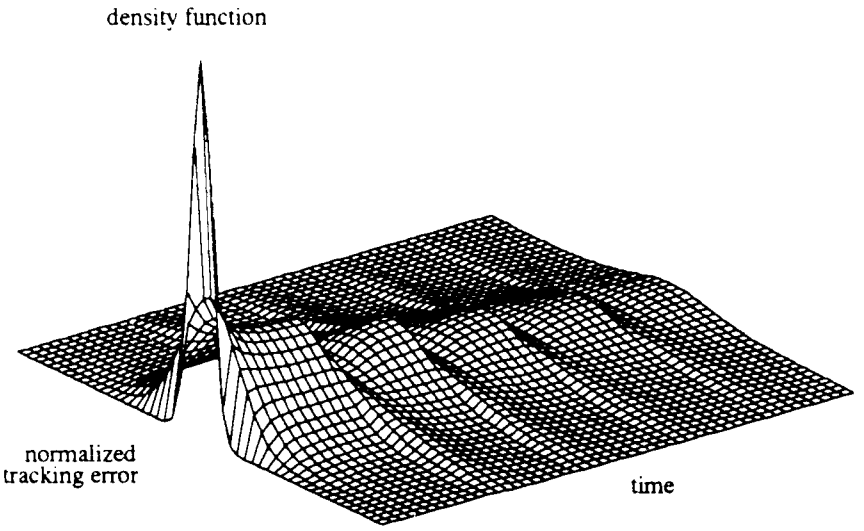

Figure 1: The 3-D plot of $p(\epsilon, t)$, for $|\epsilon| \leq 1$ and $0 < t \leq 5\tau_L$, where τ_L is the loop time constant. The initial probability density $p(\epsilon, 0) = \delta(\epsilon)$. The periodic pulse jammer with period τ_L and duty factor 30% is activated after $t = \tau_L$.

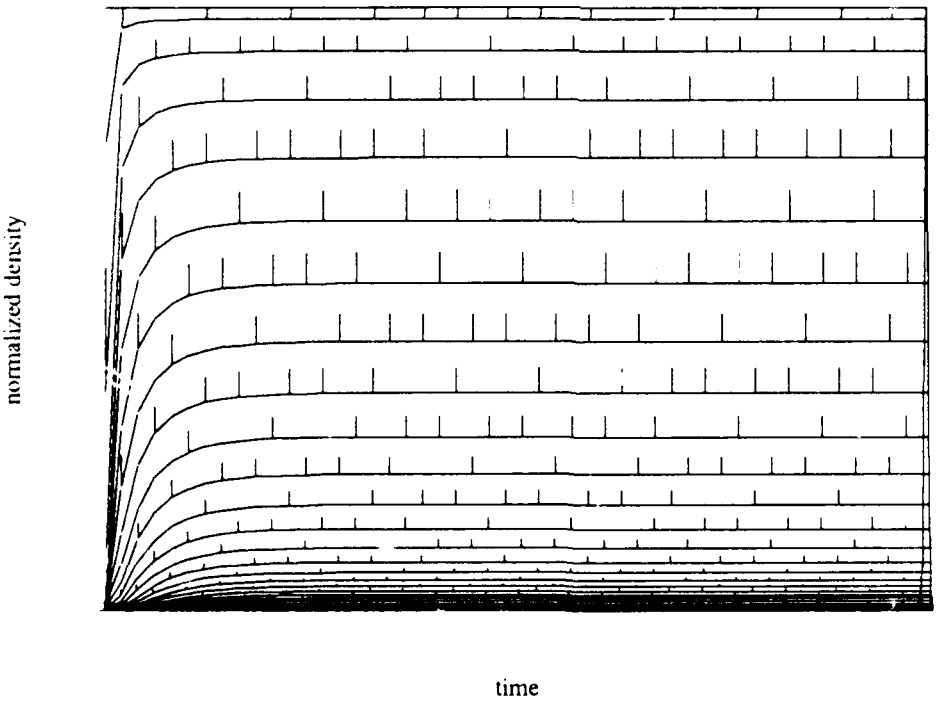

Figure 2: The side view of $p(\epsilon, t)/\max_{|\epsilon| \leq 1} p(\epsilon, t)$ for $0 < t \leq 5\tau_L$. There is no switching between jammer on-off states in this case. It shows that the cross-sections of this normalized density function at different times approach a steady state.

Basic Research In C^3 Distributed Databases

Victor O.K. Li
IE3-2

PROGRESS

In the past year, we have focused on distributed database concurrency control algorithms, failure recovery protocols, and their performance analyses. The Unified Model for Concurrency Control Algorithm, described in Pub. 6, provides a framework with which one can study and evaluate the performance of different concurrency control algorithms. In Pub. 2, a performance model has been developed for locking algorithms which incorporates the effect of deadlocks. We found that the traditional approach of resolving deadlocks by aborting transactions is extremely costly. Therefore, we have developed a new abortion-free deadlock detection-resolution algorithm (Pub. 4). In addition, we found that existing models invariably assume independent, uniform data access, i.e., each data item in the data base is equally likely to be accessed, and transactions access data items independently. In reality, this is not true. Some data items may be more popular than others, and transactions may access certain groups of data simultaneously. In Pub. 7, we have developed a general model of data access. This will allow us to develop more accurate performance models. In the area of failure recovery, we have developed replication control protocols (Pub. 3) and termination protocols (Pub. 5) in distributed databases managed on networks with unreliable components. We have also developed the domain-specific semijoin for distributed query processing (Pub. 1).

PUBLICATIONS

1. Chen, J.S.J. and Li, V.O.K., ``Domain-Specific Semijoin: A New Operation for Distributed Query Processing.'' To appear in *Information Sciences*.

2. Shyu, S.C. and Li, V.O.K., ``Performance Analysis of Static Locking in Distributed Database Systems,'' *IEEE Trans. on Computers*, Vol. C-39, No. 6, June 1990, pp. 741--751.

3. Huang, C.L. and Li, V.O.K., ``Regeneration-Based Multiversion Dynamic Voting Scheme for Replicated Database Systems,'' *Proc. IEEE International Conference on Distributed Computing Systems*, Paris, France, June 1990, pp. 370--377.

4. Shyu, S.C., Li, V.O.K., and Wang, C.P. ``An Abortion-free Distributed Deadlock Detection/Resolution Algorithm,'' *Proc. I EEE International Conference on Distributed Computing Systems*, Paris, France, June 1990, pp. 167--174.

5. Huang, C.L. and Li, V.O.K., "A Quorum-Based Commit Protocol and its Termination Protocol for Distributed Database Systems," submitted for publication.

6. Wang, C.P. and Li, V.O.K., "A Unified Model for Distributed Database Concurrency Control Algorithms," submitted for publication.

7. Banerjee, S. and Li, V.O.K., "A General Model for Non-Uniform Data Access in a Database," submitted for publication.

Segmentation and 2-D Motion Estimation of Noisy Image Sequences

A. A. Sawchuk
IE3-3

PROGRESS

We have continued work on two of the most important problems in scene analysis of image sequences: the segmentation of image frames into moving and non-moving components; and the 2-D motion estimation of the moving parts of the scene. This work involves the processing of sequences of images, a problem involving a great deal of computing due to the massive amount of frame-oriented data. In the future, we plan to shift the focus of this project to the use of smart pixel optoelectronic systems to solve such massive computation problems.

The segmentation and the motion estimation are strongly related to each other because the motion is a cue to the segmentation and the motion estimation is improved in a well segmented image sequence. We have developed an algorithm which is based on this interdependent relation. Our algorithm has two parts: segmentation and 2-D motion estimation. These parts are interactively connected in a mutually beneficial way.

The segmentation algorithm is a boundary estimation algorithm which performs well in a very noisy environment and does not require any *a priori* knowledge of the shape of the boundary [1], [2]. The algorithm is composed of three parts: (a) estimation of the boundary area (an area in which the boundary lies) , (b) minimum mean square estimation of the boundary using as *a priori* information the estimated boundary area, and (c) boundary smoothing taking advantage of the correlation of the adjacent boundary pixels. The boundary area is estimated by using the motion prediction information from the previous frames. For the first two frames

where this information is not available we use a smoothing and thresholding technique.

Our motion estimation algorithm [3] is a feature-based method with the boundary as the matching feature. The algorithm uses boundaries that have been previously estimated by the segmentation algorithm, and minimizes an objective function which depends on the mismatch between the boundary of the moving object in two consecutive frames. The optimum parameters of a motion model are found by minimizing this objective function.

These estimated motion parameters are used to predict the motion between the current and the next frame, and this information is used to improve the segmentation phase. The performance of the algorithm under different levels of noise has been examined using simulated and real images corrupted by additive white Gaussian noise. The combined algorithm can be used in applications such as image sequence enhancement and restoration, target tracking, 3-D motion estimation, motion-compensated coding, etc.

The results of this procedure have been applied to noise suppression and enhancement of a very noisy sequence of images of a moving object [4], [5]. After finding the path of motion of a segmented object from a frame sequence, smoothing or filtering is performed over a set of pixels with the same space coordinates, so that the moving parts are not blurred. We have used mean and median filters as low-pass filters and examined the performance of mean filters for different SNR (Signal-to-Noise Ratio) and different kinds of motion. Mean filtering is more effective in the case of white Gaussian noise and median filtering is more effective in the case of salt-and-pepper noise and burst noise. When using spatiotemporal filters, the spatial filtering is not performed over the boundaries because their positions are provided by the segmentation part, therefore, the edges are not blurred.

Overall, the motion compensated enhancement algorithm performs very well in a very noisy environment. This algorithm can be used for image sequence quality improvement in industrial, commercial and medical applications as well as a preprocessing step for other operations such as recognition and tracking of moving objects.

With recent advances in the technology of optoelectronic integration, arrays of light detectors, emitters, modulators can be combined with electronic signal processing circuitry on a single substrate to make "smart pixel" optoelectronic devices. These devices can be thought of as powerful generalizations of optical logic devices or spatial light modulators. Our new thrust in this work is to devise new optical architectures which make use of these devices to solve important interconnection and computing problems such as image sequence analysis. Other applications include: image understanding; neural systems; fiber-optic transmitters, receivers and switching; and parallel computing in general.

Optoelectronic technology has advanced so that the integration of optical detectors, light emitting devices, bistable optical switches and modulators with electronic gates, amplifiers and switches is possible [6]. These devices can be made in large 2-D arrays of individual elements, and the elements can serve as light modulators, light amplifiers, and threshold arrays. Each of these array elements can be denoted as a "pixel," in the sense that each can serve as a resolution cell of an image impressed on the device. These "smart pixel" or enhanced optoelectronic array devices can combine the best advantages of optics with electronics at pixel level resolution.

With the present state of technology, optics is better suited to long distance interconnections (distances greater than a few microns) because of its superior impedance matching, power dissipation and crosstalk suppression characteristics [6]-[8]. On the other hand, electronics can implement power efficient optical gates and signal amplification. Smart pixel devices are intended to make best use of these complimentary capabilities in a single materials family. The

electronic gates would perform the local logic operations at each pixel, while the optical sources and detectors would perform input/output and make the long length interconnections to distant pixels on the chip. GaAs and other III-V materials families are needed to implement high speed optoelectronic functions in a single device.

Some specific examples of optoelectronic devices that can be made in an array are: Honeywell work on an optoelectronic cellular array chip [9]; SEEDs (self electrooptic effect devices) which are electronically biased optically controlled switches being built at AT&T Bell Laboratories [10], the optical etalon array, the NEC VSTEP device, which is a light triggered pnpn thyristor [11], and work at the Jet Propulsion Laboratory (JPL) on planar LED arrays having integrated electronic drivers.

In the past, these devices have been generally made to have pixels with stable, repeatable characteristics, such as an threshold function (for optical logic) or an amplifying function (for linear optical signal processing). In some of these devices, a multiple quantum well (MQW) structure is provided at each pixel, which serves as both detector and modulator. In other devices, a separate detector and modulator structure is provided for each pixel.

Figures 1 and 2 show some concepts for an optoelectronic cellular image processing array using "smart pixel" devices. Each large square in Fig. 1 is an individual optoelectronic processing element (PE), each with its own source and one or more detectors. The PEs are shown in an array with local interconnections to the four nearest neighbors (left, right, up, down). In reality, these short distance interconnections would be done by electrical connections, leaving the longer distance connections to optics.

Figure 2 shows in detail how a shift-invariant hologram can be used with the smart pixel

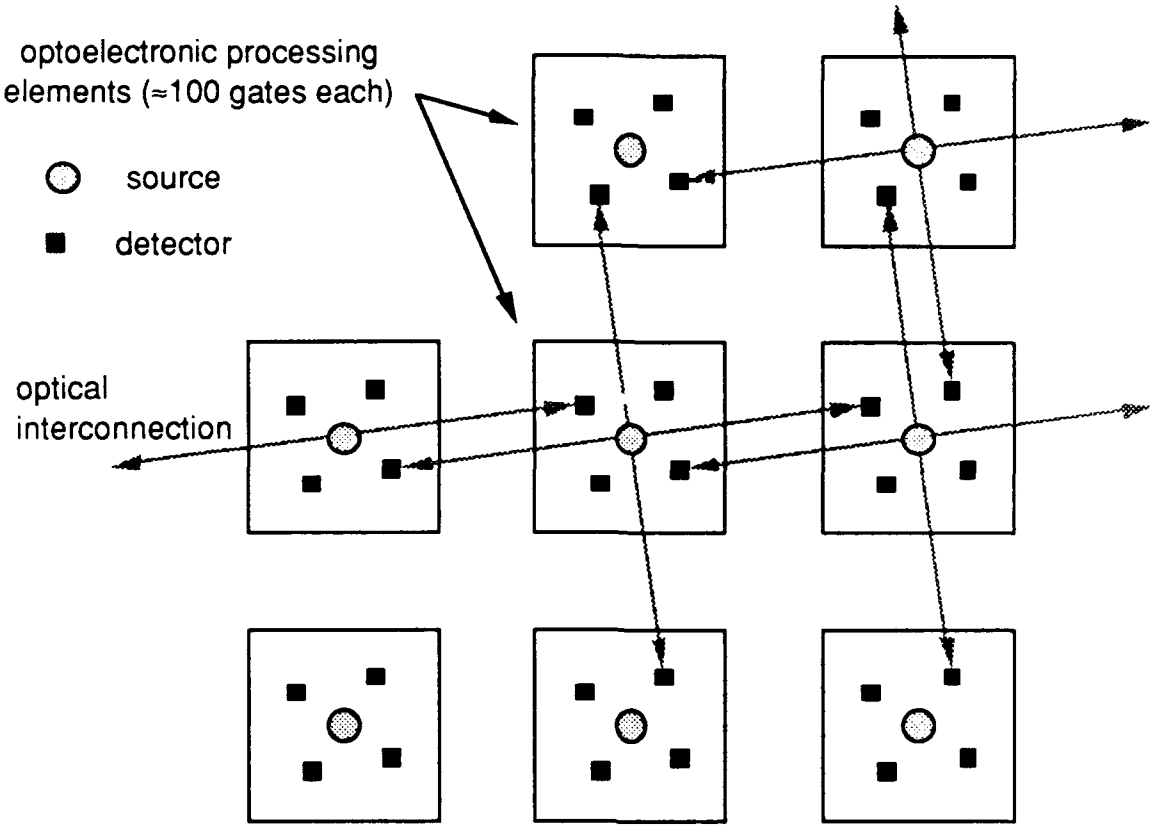

Figure 1. Cellular array implementation with a smart pixel optoelectronic chip.

SLM of Figure 1 to implement a digital optical cellular image processing (DOCIP) system which has been previously been developed as a high performance optical parallel computer [12]-[13]. Each PE in the DOCIP system has simple logic and arithmetic functions, and the operation of the array is directed from a master controller so the system operates as a single-instruction multiple-data (SIMD) processor. Much better performance can be obtained with a cellular hypercube interconnection mesh, in which there is a direct connection between any pair of processors whose labels differ in exactly one binary bit position. At the left in Fig. 2 is a *transmissive* smart pixel array. The source (output) side is imaged to the input (detector) side via an optical feedback path and a shift-invariant hologram. The hologram provides identical, shift-invariant interconnections at each pixel (processor) to form an optoelectronic implementation of a DOCIP-hypercube system.

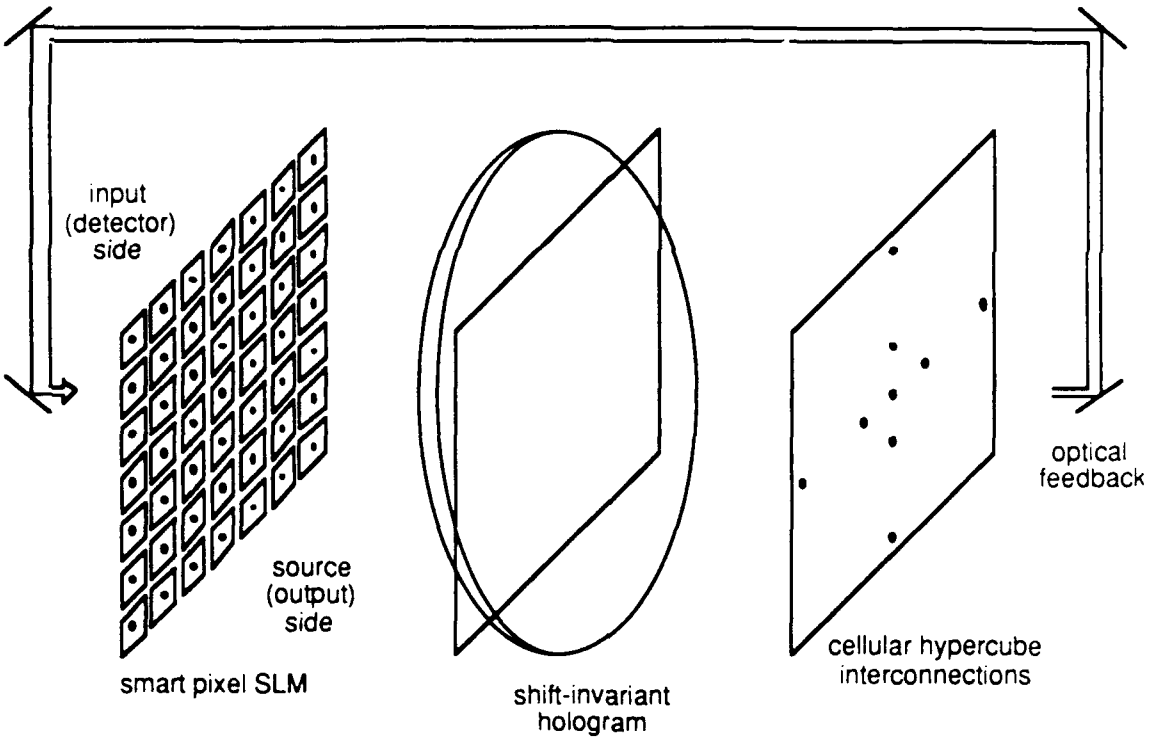

Figure 2. Combining a transmissive smart pixel SLM with optoelectronic interconnections.

Here, each processor would require on the order of 100 electronic gates to provide local memory, instruction decoding and communication to other PEs.

We have taken an overview of optoelectronic integration technology and devices and examined different computing functions that can be achieved with them. We have initially concentrated on better defined architectures such as the DOCIP system and multistage interconnection networks. Then we will look at new architectures that could be made with advanced smart pixel SLMs. The eventual goal is to determine what parts of a given system are better implemented electronically or optically.

Our approach is to compare alternative technologies on the basis of power dissipation, switching time (speed), size, packing density, scaling to larger arrays, and crosstalk for various applications. The

packing density may be determined by power dissipation, by photonic crosstalk (diffraction or aberrations in optical or holographic elements), or by electrical crosstalk (capacitive coupling, inductive coupling, or leakage currents) that occur between individual devices. A particular topic of interest is to compare the signal processing rate and power dissipation of volume (3-D structure) optical systems (characterized by the parallel interconnection of 2-D planes) versus a stack of fundamentally planar (2-D) electronic or optoelectronic processing devices which might perform the same operation. Other factors we consider are the scaling of these results as a function of increasing bandwidth (data rate) and number of parallel processing elements. The final goal is to devise improved architectures that are a better match to the constraints of a given smart pixel device technology.

PUBLICATIONS

1. D.S. Kalivas, "Segmentation and Estimation of Noisy Image Sequences", Ph.D. dissertation, University of Southern California, Los Angeles, CA, December 1989.

2. D.S. Kalivas and A.A. Sawchuk, "Object Boundary Estimation in Noisy Images," submitted to *IEEE Transactions on Pattern Recognition and Machine Intelligence*, June 1989.

3 D.S. Kalivas and A.A. Sawchuk, "A Region Matching Motion Estimation Algorithm," submitted to *Computer Vision, Graphics and Image Processing*, December 1989.

4. D.S. Kalivas and A.A. Sawchuk, "Segmentation, Motion Estimation and Enhancement of Noisy Image Sequences," submitted to *IEEE Transactions on Pattern Recognition and Machine Intelligence*, October 1990.

5. D.S. Kalivas and A.A. Sawchuk, "Motion Compensated Enhancement of Noisy Image Sequences," presented at *IEEE 1990 International Conference on Acoustics, Speech and Signal Processing*, Albuquerque, NM, April 1990.

6. S.R. Forrest, "Optoelectronic Integrated Circuits," Invited Paper, *Proc. IEEE* , vol 75, p. 1488 , 1987.

7. D.A.B. Miller, "Optics for Low-Energy Communication Inside Digital Processors: Quantum Detectors, Sources, and Modulators as Efficient Impedance Converters," Optics Letters, vol. 14, pp. 146-148, 15 January 1989.

8. Y. Liu, J.G. Johnson and S.R. Forrest "Optically Powered Optical Interconnection System", *IEEE Photonics Technology Letters*, vol. 1, p.21, 1989.

9. M. Hibbs-Brenner, S.D. Mukherjee, M.P. Bendett and A.R. Tanguay, Jr., "Integrated Optoelectronic Cellular Array for Fine-Grained Parallel Processing Systems," *Optical Computing, 1989 Technical Digest Series*, vol. 9, pp. 223-226, Optical Society of America, Washington, DC, (1989).

10. D.A.B. Miller, "Optoelectronic Applications of Quantum Wells," *Optics and Photonics News*, vol. 1, no. 2, pp. 7-15, February 1990.

11. K. Kasahara, *et al*, "Double Optoelectronic Switch as a Dynamic Memory with Low Power Consumption," *Appl. Phys. Lett.*, vol. 52, no. 9, pp. 679-681, 29 February 1988.

Ph.D. Theses

D. S. Kalivas, "Segmentation and Estimation of Noisy Image Sequences", Ph. D. dissertation, Department of Electrical Engineering, University of Southern California, CA December 1989.

Mathematical Modeling and Control of Complex Systems: Applications to Piezoelectrically Coated Large Space Structures

E. A. Jonckheere
IE3-4

PROGRESS

The inaccuracy of flexible space structure models has always been a source of concern for control engineers. Too often has it happened that, confronted with the gross uncertainty on the structure model, the design engineer opted for an overly robust design, deliberately sacrificing such mission-oriented specifications as disturbance rejection, pointing accuracy, etc.

To be more precise, the fundamental limitation on the achievable performance reads

$$S(j\omega) + T(j\omega) = I$$

In the above, S is the **sensitivity** *function* that *measures such mission-*oriented specifications as disturbance rejection, shape control, vibration isolation, pointing accuracy, etc. On the other hand, T is the **complementary sensitivity** yielding a measure of the amount of model inaccuracy that the loop can sustain. If $\hat{G}(s)$ is the structure **model**, and if the transfer matrix of the real structure is written as $\hat{G}(I+\Delta)$, then the maximum allowable size for Δ is given by the frequency response inequality

$$\|\Delta\|_\infty < \frac{1}{\|T\|_\infty}$$

From this elementary analysis, it follows that, if model uncertainty Δ is reduced, then T could become "bigger" and consequently S could become "smaller," resulting in the possibility of achieving tighter mission-oriented tolerances.

For our purposes, an "accurate" model is characterized by a "small" $\|\Delta\|_\infty$. Therefore, **the state space MODEL** $D + C(sI-A)^{-1}B = \hat{G}(s)$ **is "accurate" if its frequency response** $D+C(j\omega I-A)^{-1}B$ **matches the**

experimentally. It suffices to excite the electrical input of an actuator with a sine wave,

$$u_i(t) = \sin \omega_k t ,$$

measure the sine wave at the electrical output of the sensor

$$y_j(t) = r_k \sin(\omega_k t + \phi_k) ,$$

measure the gain r_k and phase ϕ_k, and get a sample of the experimental frequency response

$$(G(j\omega_k))_{ij} = r_k e^{j\phi_k}$$

Therefore, the state-space MODEL (A,B,C,D) **will be accurate for our purposes if it matches the REAL** behavior of the structure as revealed by its experimental frequency response data,

$$D + C(j\omega_k I - A)^{-1}B \cong \{r_k e^{j\phi_k}\}$$

To measure how closely the model frequency response and the experimental data match, it is convenient to define the relative error criterion:

$$\|H^{-*}(G-\hat{G})\|_\infty$$

$G(j\omega_k) = \{r_k e^{j\phi_k}\}$ = experimental data
= transfer matrix of real structure at sample frequencies

$\hat{G}(j\omega) = D + C(j\omega I - A)^{-1}B$ = reduced order state space model

and H is the spectral factor

$$H^*H = GG^*$$

The relative error approach to model matching was introduced by Glover and Jonckheere [1985]. Observe that the matching criterion can be rewritten

$$\|H^{-*}G - H^{-*}\hat{G}\|_\infty$$

and it should be clear to those familiar with modern Hankel and L^∞ norm theory that the **crucial** issue in this modelling problem is the **Hankel Operator induced by the matrix** $H^{-*}G$. The matrix $H^{-*}G$ has been referred to as **phase matrix** by Glover and Jonckheere [1985]. This terminology stems from the easily proved fact that $H^{-*}G$ is **unitary**. Glover and Jonckheere [1985] developed a solution to the relative model matching problem -- in the case where $H^{-*}G$ is **completely specified**, i.e., $H^{-T}(j\omega)G(j\omega)$ is specified over the entire continuum of frequencies, $\omega \in \mathcal{R}$, or equivalently, a transfer function or state-space model for $H^{-T}(s)G(s)$ should be available. In a few words, the solution goes as follows: Let $K(s)$ be the causal (stable) part of $H^{-T}(s)G(s)$. Let $\hat{K}(s)$ be the usual balanced or Hankel-norm reduced order causal model of $K(s)$. Then $\hat{G}(s)$ is found to be the causal part of $H^{-T}(s)\hat{K}(s)$. Furthermore, let $\sigma_0 \geq \sigma_1 \geq \sigma_2 \geq \ldots$ be the Hankel singular values of the causal part of $H^{-T}(-s)G(s)$. If $\hat{G}$ has degree d, then the quality of the matching can be assessed from

$$||H^{-*}(G-\hat{G})||_\infty \leq (1 + \sigma_d)(1 + \sigma_{d+1}) \ldots$$

In our problem of **identification from experimental phase/gain data**, the difficulty is two-fold. First, we only have an **incomplete** description of $H^T(-j\omega)G(j\omega)$, the latter frequency response could only possibly be known at finitely many sample frequencies ω_k. Secondly, all we know from experiment is the sampled frequency response $G(j\omega_k) = \{r_k e^{j\phi_k}\}$ and one still has to construct $H^{-T}(-j\omega_k)G(j\omega_k)$ from the experimental data.

Recently progress has been made along the lines of these two technical difficulties. Regarding the construction of the phase matrix H^*G from experimental Bode plots, some FFT procedures have been devised. However, over the past few years, the split radix fast Hartley transform has proved faster than the conventional FFT and we have therefore developed a split radix fast Hartley transform approach to this problem. Regarding the accuracy of the identification procedure between sample frequencies, we have found that the theory of the width of an analytic function provides some error bounds.

PUBLICATIONS

Ph.C. Opdenacker, E. A. Jonckheere, et al., "Reduced-order compensator design for a flexible structure," Journal of Guidance, Control and Dynamics, Vol. 13, pp. 46-56, January-February 1990.

E. A. Jonckheere and Chingwo Ma, "Split radix fast Hartley transforms in one and two dimensions," IEEE Transactions on Acoustics, Speech and Signal Processing, February 1991.

TYPICAL CLOSED LOOP PERFORMANCE ON FUNDAMENTAL MODE OF 10 INCH BEAM

(MAXIMUM INPUT VOLTAGE = 100 V)

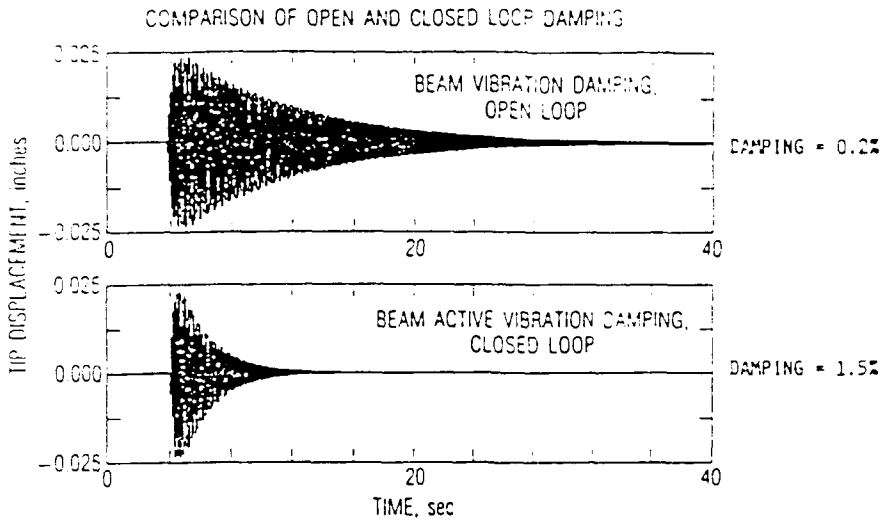

Open and closed loop time response of single PVDF segment beam.

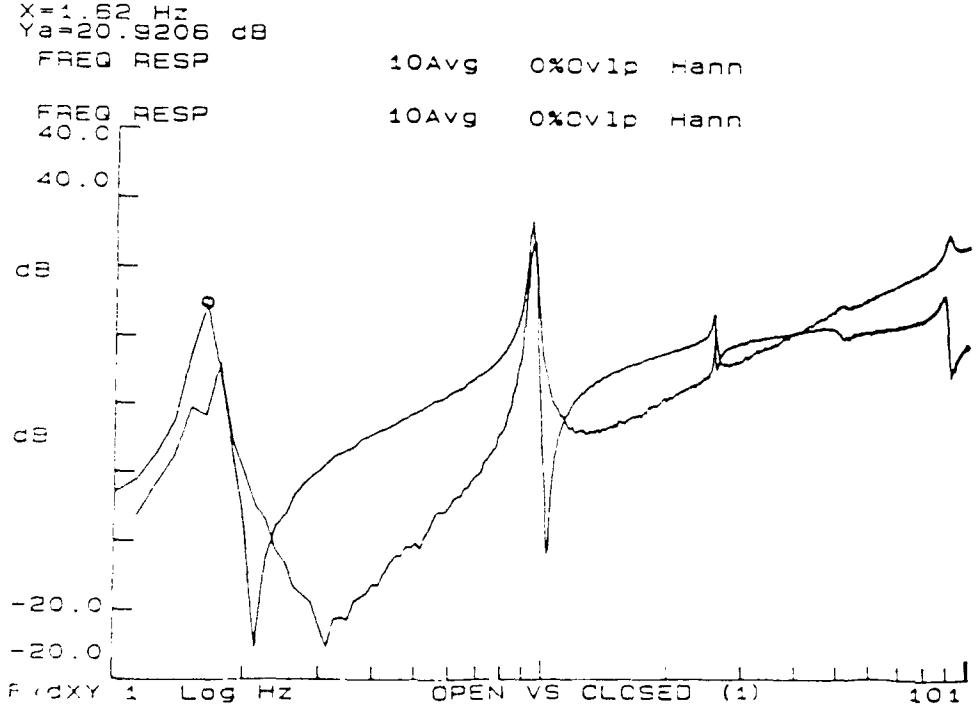

Open and closed loop transfer function of four segment beam.

Distributed Actuation and Sensing Concept

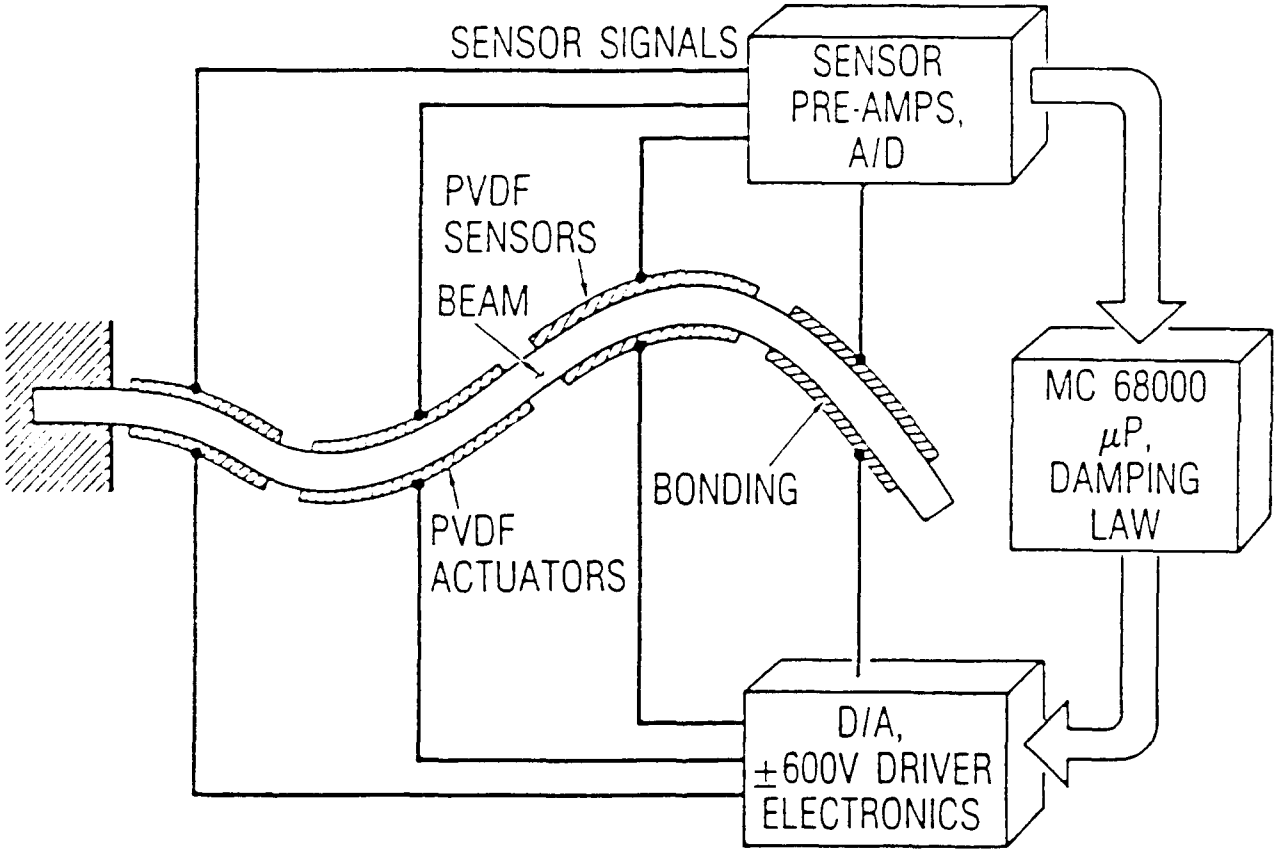

Knowledge Based Interpretation of Aerial Images

R. Chellappa
IE3-5

PROGRESS

The goal of this research project is to develop a general framework for knowledge based interpretation of a class of aerial images. During the calendar year 1990, we have made several important contributions to the problem of matching a stereo pair of aerial images. Specifically, we have developed a hierarchical approach, wherein progressively finer features are matched to measure the disparity between the two views. The hierarchical approach is more robust than an approach using a single set of features. The hierarchy consists of lines, vertices, edges and edge-rings.

Matching starts at the highest level of the hierarchy (edge-rings) and proceeds to the lowest (lines). Higher level features are easier to match, because they are fewer in number and more distinct in form. These matches then constrain the matches at lower levels. The system evolves dynamically as new match hypotheses are added and those that violate certain geometric constraints are deleted. A TMS (Truth Maintenance System) is used to maintain the consistency of the database and carry out the logic revisions necessitated by additions, deletions and confirmations of hypotheses. Excellent real image results have been obtained. Figures 1 through 8 present typical results.

PUBLICATIONS

1. V. Venkateswar and R. Chellappa, " Extraction of Straight Lines in Aerial Images," *Signal Processing V: Theories and Applications*. L. Torres, E. Masgrau and M.A. Lagunas (eds.), elsevier Science Publishers, pp. 1671-1674, 1990.

2. V. Venkateswar and R. Chellappa, "A Framework for Interpretation of Aerial Images", *International Conference on Pattern Recognition (Computer Vision Track)*, Atlantic City, NJ, June 1990.

3. V. Venkateswar and R. Chellappa, "Hierarchical Stereo Matching Using Feature Groupings," (Submitted to IEEE Computer Science Conf. on Computer Vision and Pattern Recognition, Hawaii, June 1991).

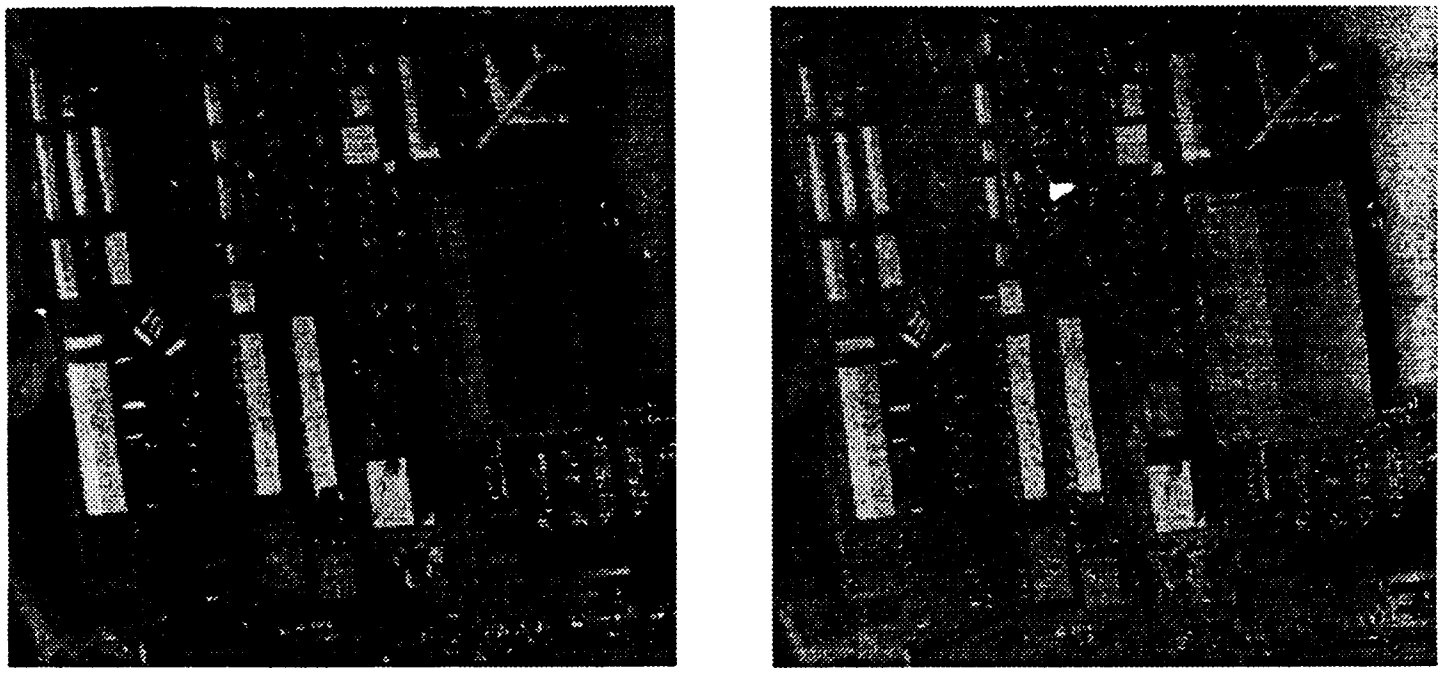

Figure 1: Stereo pair.

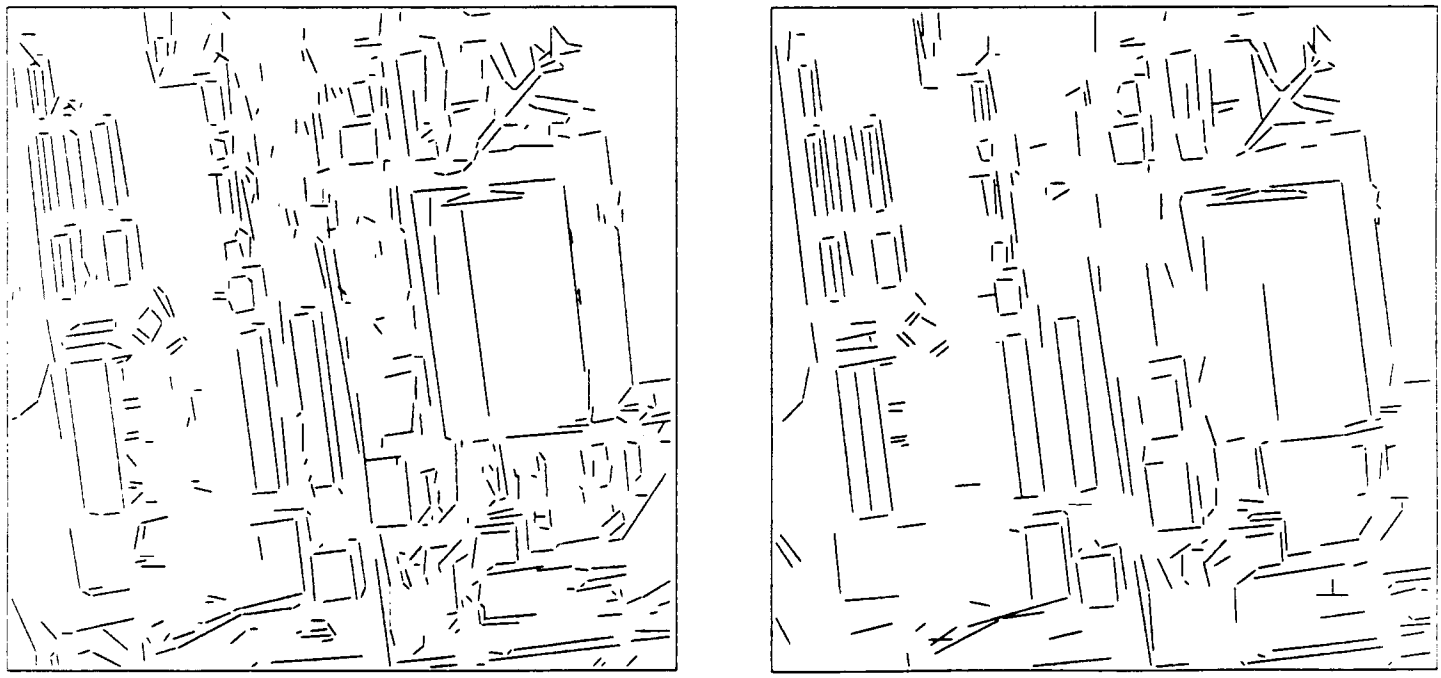

Figure 2: Lines extracted from the two views.

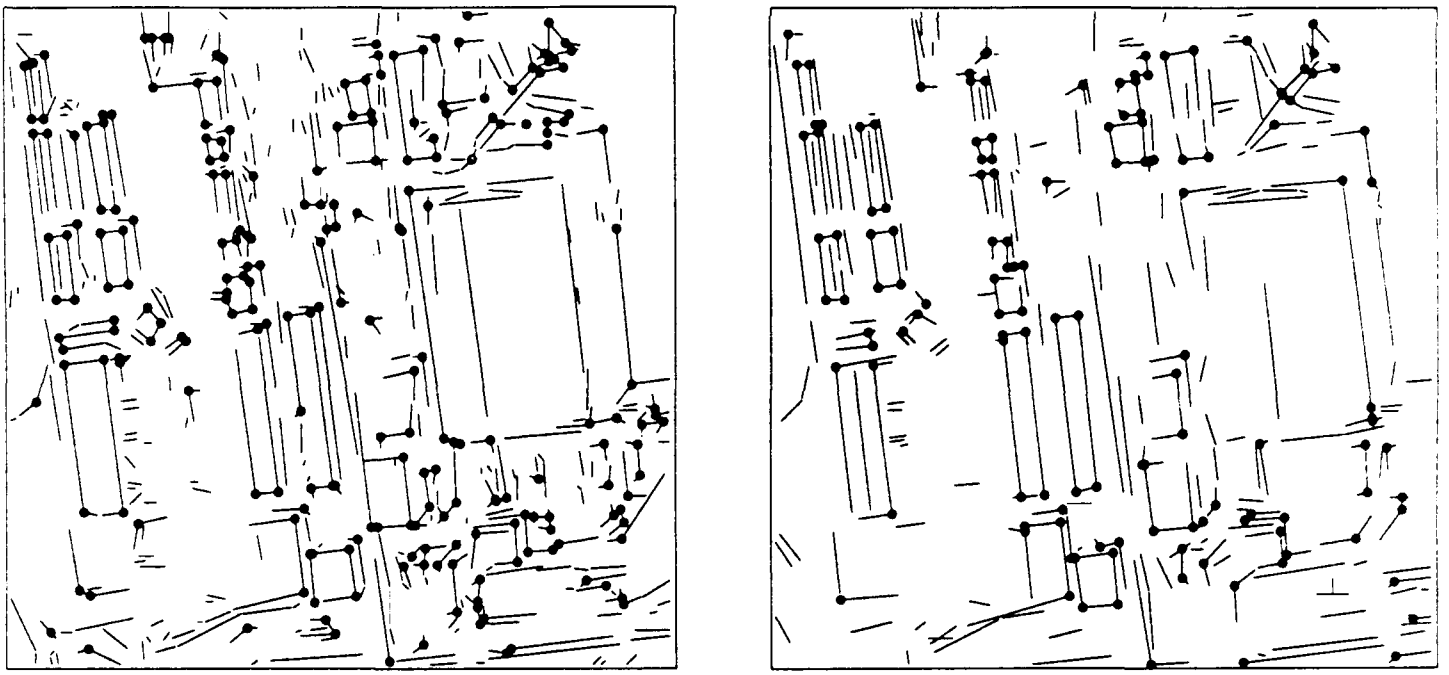

Figure 3: Vertices (dark circles)

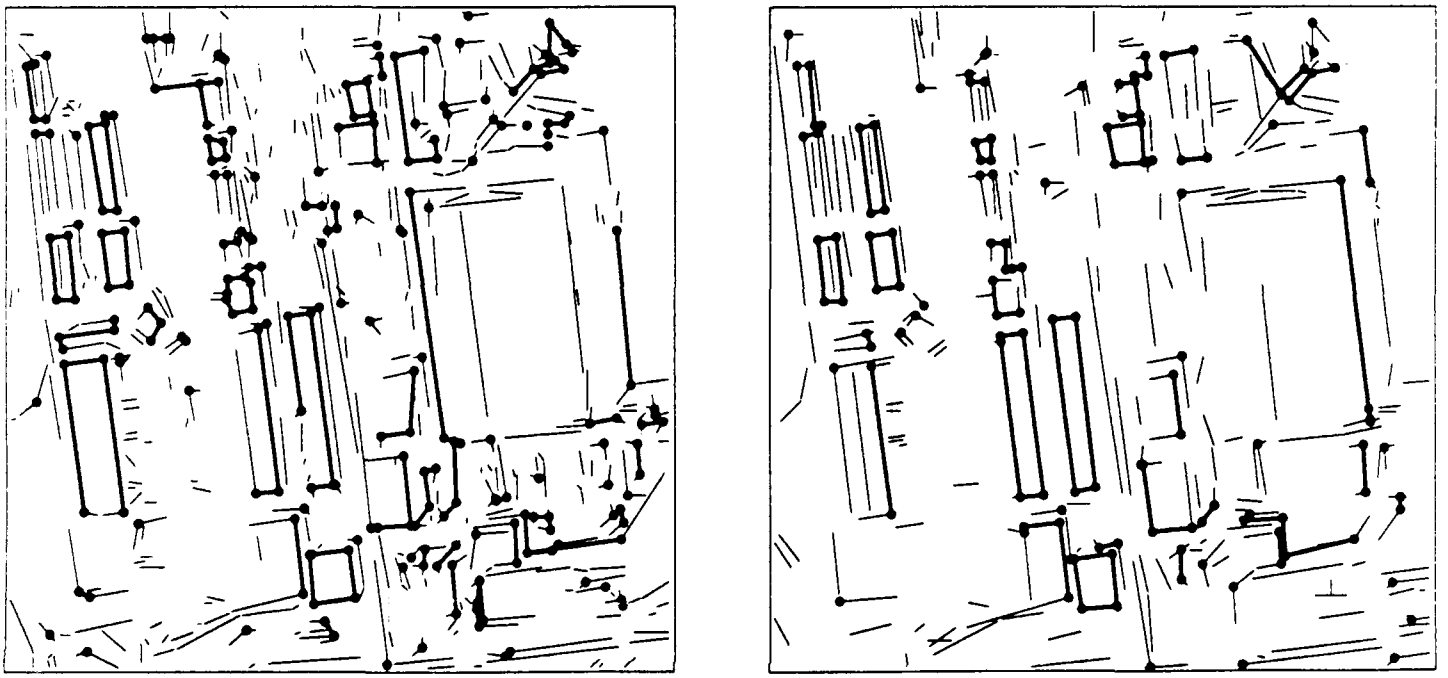

Figure 4: Edges (dark lines)

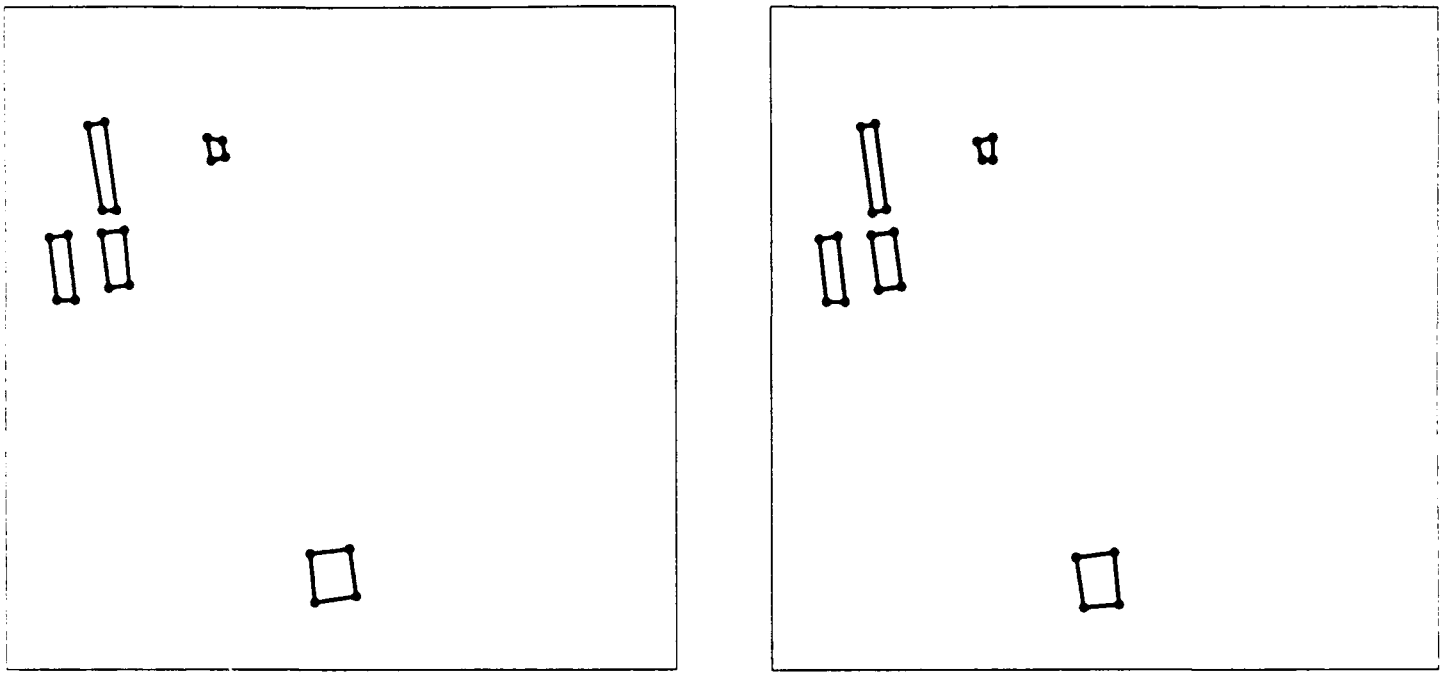

Figure 5: Matches at edge-ring level.

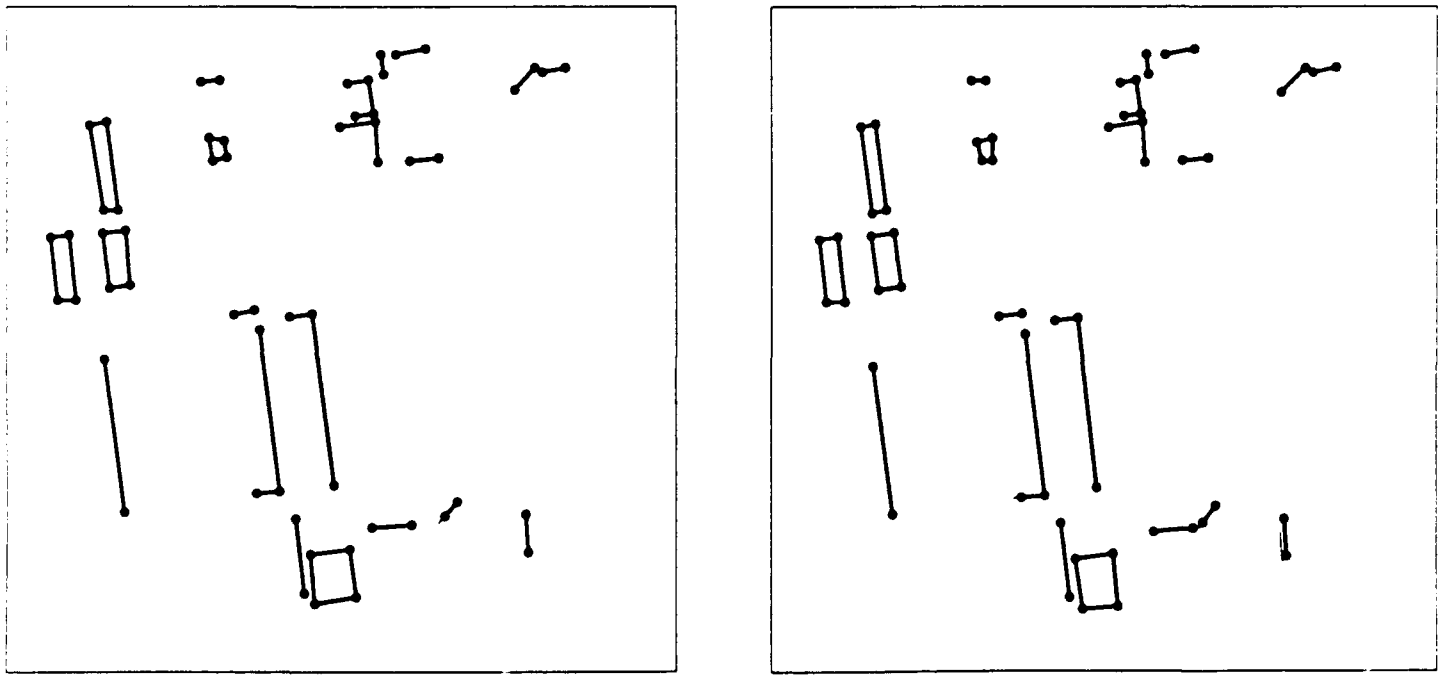

Figure 6: Matches at edge level.

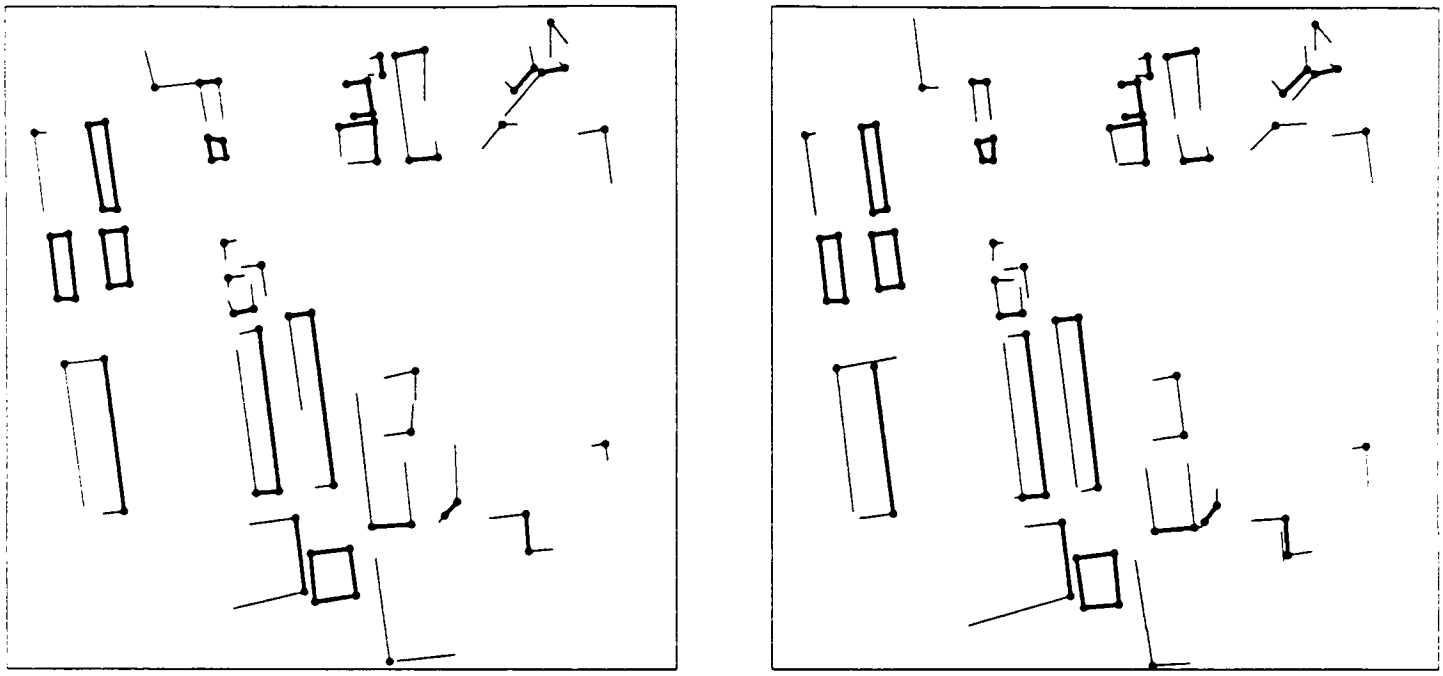

Figure 7: Matches at vertex level.

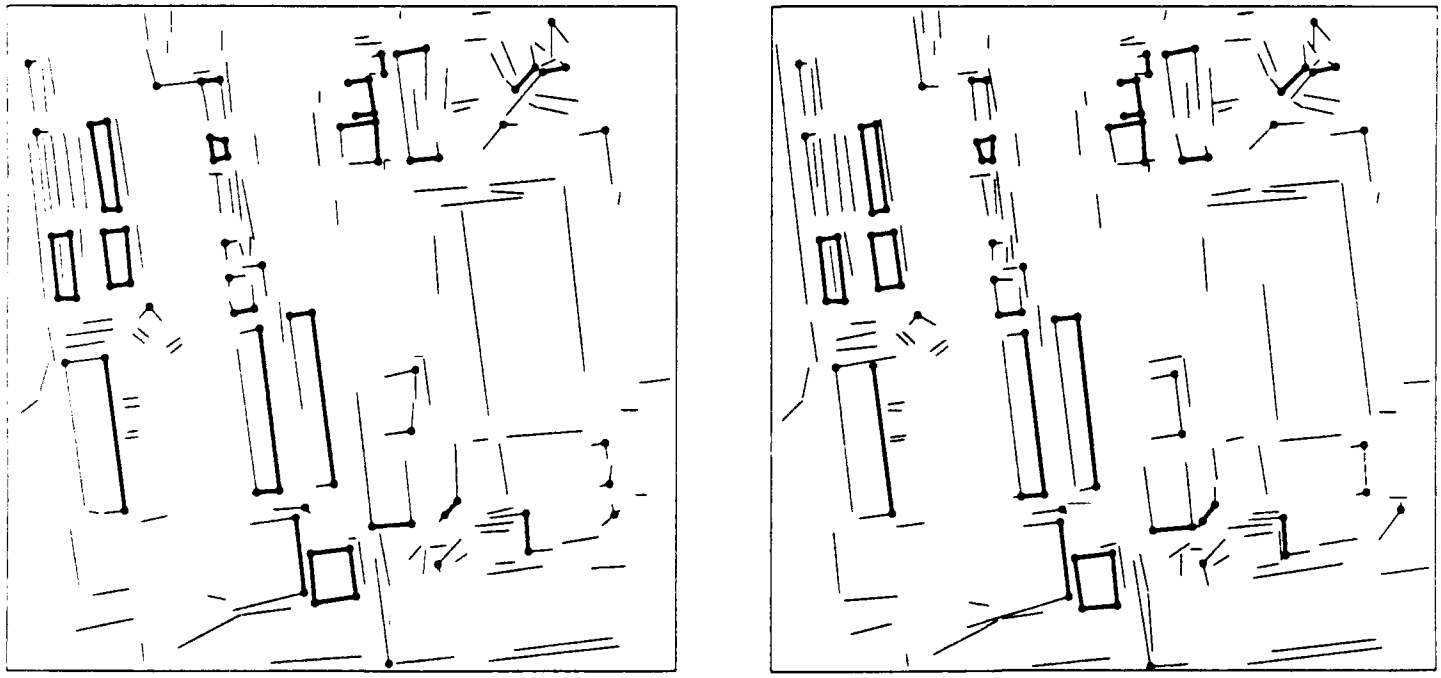

Figure 8. Final matches at line level.